Master thesis

Experimental investigation of drag propulsion on an accelerating hand for various finger spreading in human swimming

by

Etienne LE BIHAN (4844769)
e.lebihan@student.tudelft.nl

08/12/2020

Thesis committee:	Prof. dr. ir. J. Westerweel,	TU Delft, supervisor
	Ir. E.F.J. Overmars,	TU Delft, supervisor
	Dr. ir. M.J. Tummers,	TU Delft
	Dr. A. Laskari	TU Delft

P&E report number: 3038

Project duration: March 3, 2020 – December 8, 2020

Source image: blog.arenaswim.com/us/training-technique-us/alternate-breathing-perfectly-balanced-freestyle-swimming/

Acknowledgements

This work marks the end of my studies as an Energy & Process Technology master student at TU Delft. I would like to take this opportunity to thank many people for their help and guidance throughout my thesis.

First, I would like to thank ir. Edwin Overmars for his precious help all along this thesis. I am really grateful for your constant availability and all the effort you have done to make this thesis possible. Without your expertise, it would have been much more difficult to implement my experiments. I am particularly grateful that dr. ir. Jerry Westerweel gave me the opportunity to work on this very interesting topic, and for his guidance during these nine months. Furthermore, I would like to thank dr. ir. Willem van de Water for his time and his advices, especially regarding his work on the numerical calculation of the hands' characteristics. I am also thankful to Gertjan Mulder and Jasper Ruijgrok for their precious help to improve, facilitate and conduct my experiments.

E. Le Bihan
Delft, December 2020

Nomenclature

PIV	Particle Image Velocimetry
LSV	Laser Speckle Velocimetry
a	Object acceleration (m.s^{-2})
A	Projected area (m²)
C_d	Drag coefficient (-)
d_p	Density of particles (particles/m²)
D_p	Particle diameter (μm)
F_d	Drag force (N)
F_{C_d}	Steady drag force (N)
F_{vm}	Force due to virtual mass (N)
F_{mh}	Residual force (N)
Γ	Circulation (m².s^{-1})
m_{hd}	Hydrodynamic mass (kg)
m_{hn}	Hand mass (kg)
ρ_f	Fluid density (kg.m^{-3})
Re	Reynolds number (-)
V	Object velocity (m.s^{-1})
V_a	Mean velocity (m.s^{-1})
ω	Vorticity (s^{-1})

Abstract

In professional swimming, a fraction of second can determine whether a competitor will obtain a place on the podium. Swimming techniques have been analysed for decades to increase and optimize performance in order to win medals in the biggest competitions. The arms and the hands play a major role in the forward propulsion generated by a swimmer, especially in front crawl swimming. They have been widely investigated for steady motion, from the elbow position to the hand orientation and configuration. However, it is argued that the arm velocity is continuously varying during a front crawl stroke and that this unsteadiness can enhance propulsion. For this reason, investigating the effect of unsteady motion on the propulsive forces generated by the hand is of great interest. The objective of this study is to experimentally investigate the effect of acceleration on the propulsion drag of a hand in human swimming, and how this effect evolves with finger spreading. To do so, experiments on four full-scale 3D printed hands with attached forearm and different finger spreading are performed. The experiments take place in a 2 x 2 m open glass tank filled with water. The hands, mounted on a robot arm and fully submerged, are accelerated towards a constant target velocity along a linear path. The acceleration and the velocity are varied resulting in a Reynolds number of $2 \times 10^4 \leq Re \leq 6 \times 10^4$ based on the hand palm. The drag force exerting on the hand is measured as a function of time and three phases are distinguished: (i) the acceleration phase during which the drag reaches a maximum, (ii) the transition phase where the drag gradually decreases to reach a constant value during (iii) the steady phase. In parallel, two-dimensional particle image velocimetry (PIV) is performed in a plan crossing the fingers. A significant effect of acceleration was found performing experiments for four different accelerations. Higher accelerations generate stronger and more concentrated vortices behind the hand, resulting in a larger amount of circulation close to the hand. Consequently, a 25% increase is found in the drag force at the end of the acceleration when the latter is multiplied by four. No significant effect of finger spreading on the drag force during the acceleration was found. However, surprisingly, an enhancement of the drag force of 5% to 10% was measured during the transition phase and the steady phase for the closed hand compared to the hands with finger spreading. PIV showed larger amount of circulation close to the hand without finger spreading.

Contents

1. Introduction

Swimming is a discipline which consists of generating propulsion to overcome the drag exerting on the body and create a forward motion through water. For elite swimmers, the time difference between two final positions is often around a few tenths of a second or even smaller, so the gain of a fraction of a second can make a huge difference in the final result. As an example among many others, in 2008 at the Beijing Olympics Games, the French swimmer Alain Bernard won the gold medal of the 100 m freestyle by 0.11 s in front of the Australian Eamon Sullivan. That is why swimming techniques and hydrodynamics have been investigated for decades on many aspects, in order to improve the efficiency and to reach the podium of the main competitions.

In front crawling, the limbs and especially the arms play an essential role in the generated propulsion forces. The motion of the arm and the hand configuration have been particularly investigated to understand the flow mechanisms at stake and help coaches and swimmers in using optimal techniques. Many parameters have been identified and a small change in one of them can have a significant impact on the generation of propulsive forces: the hand configuration including the hand cupping, the finger spreading or the thumb position; the angle of attack; the stroke motion (S stroke, straight stroke); the velocity profile of the arm (acceleration, deceleration). Many numerical and experimental studies have been done on the subject and reviews of studies regarding hydrodynamics of swimming exist (van Houwelingen et al., 2017a; Wei et al., 2014). While Wei et al. (2014) made an overview of competitive swimming, van Houwelingen et al. (2017a) focused on hands and arms hydrodynamics. As mentioned by van Houwelingen et al. (2017a), most of the experimental work on the hydrodynamics around the hand and arm of a swimmer has been done in water or wind tunnels, so at steady motion. However, swimming strokes are strongly unsteady, it has been argued that steady hydrodynamic theory is not sufficient to describe propulsion mechanisms in swimming (Samson et al., 2017; Takagi et al., 2014a) and unsteady flow phenomena are widely contributing to the propulsion generated by a swimmer. These phenomena have been investigated by generating complex motions, with accelerations, on various objects from a flat plate (Grift et al., 2019), as a simple geometry, to full-scale arms attached to mechanical devices like robots in order to recreate conditions closer to actual swimming. Also, particle image velocimetry (PIV) has been used to look at the flow behaviour in detail. Actual swimmers participated in few studies to generate a realistic swimming stroke, but it induces a repeatability problem compared to models, and it does not enable an easy implementation of equipment for measurements. Nonetheless, the understanding of the flow behaviour and the effect of every parameter mentioned on propulsion are still not well defined.

In this thesis, the effect of acceleration on drag propulsion in swimming is investigated for different finger spreading by means of force measurements and particle image velocimetry. This chapter introduces a general description of the front crawl stroke and PIV. Then, different aspects of hand propulsion in swimming are discussed and the latest findings on each of these aspects are presented. After that, the study of Grift et al. (2019) on the drag of an accelerating

plate, from which this thesis has been widely inspired by, is reviewed. Finally, the research objectives of this thesis are formulated.

1.1. Front crawl swimming

Front crawl swimming, or free style, is probably the most common swimming stroke and has been widely investigated, especially to optimise the technique and performance. This stroke can be divided in four main phases as described in Figure 1 (Cortesi et al., 2019). The catch and entry correspond to the initial phase during which the hand enters the water. Then, the pull represents the first phase of propulsion during which the arm begins its backwards movement. At the end of the pull phase, the hand is in the transversal plan crossing the shoulder perpendicular to the water surface, and here starts the push phase, which is the second propulsive phase. The end of the pull phase does not contribute to forward propulsion and can increase the drag of the body and consequently slow down the swimmer. To avoid it, the palm of the hand is turned inward to minimize drag before the exit. Finally, the hand exits the water to start the recovery phase during which the arm is brought back forward over water to start a new cycle with the catch and entry phase. Since the pull and the push phases correspond to the propulsion part of the stroke, they represent the most interesting part to investigate and optimize.

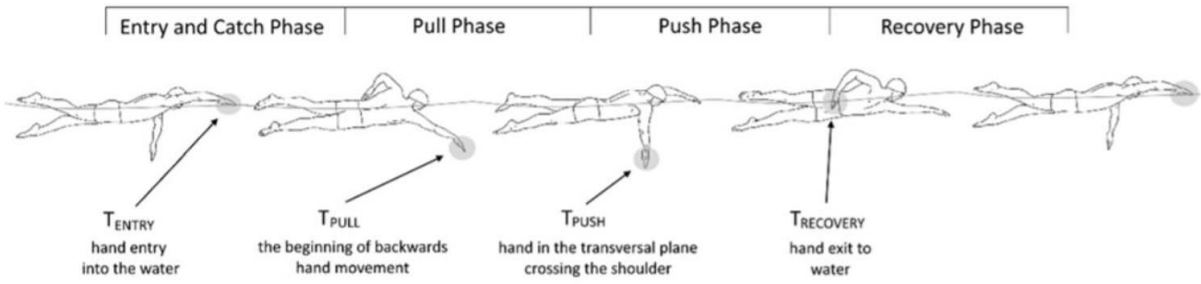

Figure 1 : Scheme of the four phases of a front crawl stroke (Cortesi et al., 2019)**.**

1.2. Particle image velocimetry

Particle image velocimetry (PIV) refers to methods used in experimental fluid mechanics to determine the instantaneous velocity field by measuring the displacements of fine particles that accurately follow the motion of the fluid (Adrian & Westerweel, 2011). Many PIV techniques have been developed since its first use, from planar PIV using a single camera system to three-dimensional PIV using a more complex system. Initially used in solid mechanics, laser speckle velocimetry (LSV) is a technique close to PIV, which determines the displacement of speckle patterns instead of particles, but PIV remains the main method to determine velocity fields in fluid mechanics since it has been argued that particles density are rarely large enough to create speckles (Adrian & Westerweel, 2011). PIV provides a qualitative visualisation of the flow, and so it enables observation of the effect of small modifications in the investigated flow (Adrian & Westerweel, 2011), especially the flow around objects. In this

way, PIV has been widely used for the investigation of swimming techniques, particularly to study the flow around the hands during strokes. PIV has been used in this thesis to accurately study the hydrodynamics around the hand during and after acceleration, for different finger spreading.

1.3. Drag in swimming

The drag force of an object in steady motion F_d is traditionally defined as:

$$\boldsymbol{F_d = \frac{1}{2}\rho_f V^2 C_d A} \quad \textbf{(1)}$$

with ρ_f the fluid density, V the object velocity, C_d the dimensionless drag coefficient and A the projected area of the object.

There are two drag forces in swimming: the drag of the body, undesirable, that needs to be overcome, which resists against the forward motion of the swimmer through the water, and the propulsion drag generated by the stroke that pushes the swimmer forward. The latter is exerted in the opposite direction of the motion, and therefore induces forward propulsion of the swimmer. As explained by van Houwelingen et al. (2017a), more than 80% of the propulsion in swimming is generated by the arms, and the hands are responsible for more than 70% of arms propulsion which make them particularly interesting in the investigation and the optimisation of drag in swimming.

The drag of an object can be divided in three main components: (i) the pressure drag due to pressure difference around the object, (ii) the viscous drag (or friction drag), predominant in low velocity flows, due to the viscosity of the fluid and the formation of boundary layers around the object, and finally, (iii) the wave drag in presence of a free surface. The drag to overcome includes friction drag between the body and the water that can be reduced by wearing a swimsuit, the pressure drag that is minimized by keeping the body as straight as possible to reduce the frontal area, and the wave drag due to surface waves produced by the swimmer. The propulsion drag is mostly generated by the pressure drag, so the pressure difference around the limbs, in particular the hands, and therefore can be strongly affected by small changes in different aspects of the hands motion.

1.3.1. Finger spreading

According to van Houwelingen et al. (2017a), few studies investigated the effect of finger spreading on propulsion, both numerically and experimentally. Schleihauf (1979), one of the first to study the effect of finger spreading in swimming, made experiments in a water channel on three different finger spacing finding a higher drag coefficient for closed fingers. Marinho et al. (2010) as well as Minetti et al. (2009) and Bilinauskaite et al. (2013) performed numerical simulations at steady motion. The first two studies found an increase in C_d for a small finger spreading, and the last study concluded that a larger drag force is generated for a spread hand rather than a closed hand, due to higher pressure forces. Lorente et al. (2012) modelled fingers

as cylinders and found an optimal finger spreading based on the interaction between individual finger's boundary layer.

Van Houwelingen et al. also worked on the effect of finger spreading on drag for steady motion (van Houwelingen et al., 2017b), using the exact same models for numerical and experimental study, since 3D printed models were manufactured from the numerical hands used in the simulation. The experiments were done in a wind tunnel and showed a maximum C_d at a 5° finger spreading and an approximated division of the forces on the hand and forearm gave a maximum drag for the hand alone at 10° finger spreading whereas the simulations showed maxima at 10° and 20° finger spreading for both cases: hand and forearm and hand alone (see Figure 4 in section 2.2 for the definition of the finger spreading angles). Bazuin (2018) also investigated the finger spreading using the same models in a towing tank at stationary state and found an optimal propulsion drag for a 5° finger spreading with up to 1.7% larger drag than the closed hand.

From most of the studies and as highlighted by van Houwelingen et al. (2017a), it appears that a small finger spreading can induce higher propulsive forces by increasing the drag coefficient C_d. However, most of these studies have been done for stationary flow while actual swimming strokes include accelerations and decelerations of the arm and hand, particularly front crawl.

1.3.2. Thumb position, angle of attack and cupping

Various studies investigated different hand configuration parameters such as the thumb position, the angle of attack or the cupping of the hand. On the thumb position, two cases have been defined: the abducted thumb, which corresponds to an open thumb away from the hand palm and the adducted thumb, when the thumb is close to hand palm. The results diverged on the thumb position: Marinho et al. (2009) found a higher drag for the adducted position, while van den Berg et al. (2018) found a higher drag for the abducted thumb. Also divergence was found in the results for the angle of attack: a maximum drag was found when the hand is perfectly perpendicular to the flow in some studies (Schleihauf, 1979) and when there is a slight angle with a leading thumb in other studies (van den Berg et al., 2018). Finally, in most of the studies it has been argued that a flat hand generates a higher drag than a cupped hand since it gives a bigger projected area although a cupped hand is expected to increase C_d (van den Berg et al., 2018).

1.3.3. Front crawl unsteady motion

Most of the experimental work on swimming hand and arm motion including the acquisition of fluid forces and dynamics using PIV investigated steady flow conditions. However, the complex motion of swimming strokes like front crawl induces unsteady hydrodynamic phenomena, which appear to strongly contribute to propulsion as showed by Takagi et al. in the investigation of unsteady sculling motion (Takagi et al., 2014b). They highlighted the important role of unsteady vortices like leading-edge vortices (LEV) and the interaction between the hand and these vortices, called wake capture phenomena, in the production of propulsive hydrodynamic forces.

As mentioned before, all swimming techniques consist of complex motions, so the velocity of the arm and hand is not constant during a full swimming stroke, especially during the propulsion phase. The motion contains accelerations and decelerations. As mentioned by Bazuin (2018), van Houwelingen captured the path of one hand motion during a front crawl stroke (Figure 2). From this, he estimated the average velocity V_a during the propulsion phase of a front crawling stroke as $V_a = 1.5$ m/s, with the maximum velocity reached being around 2 m/s.

Figure 2 shows a wide range of accelerations up to 12 m/s². Mooney et al. (2015) measured accelerations up to 40 m/s² on a swimmer's wrist during a front crawl stroke using a kinematic sensor. Gourgoulis et al. (2015) estimated accelerations up to 27 m/s² by means of a multiple cameras set-up. Despite differences in the figures mentioned, it shows how significant accelerations are during an actual swimming stroke.

A few studies, mostly numerical, investigated the effect of acceleration on drag propulsion generated by the hand in human swimming (van Houwelingen et al., 2017a). They all indicated that hand accelerations could increase the propulsive forces compared to steady hand motion. In particular, Kudo et al. (2013) suggested that the unsteady flow caused by acceleration induces the generation of vortex that enhances propulsive forces.

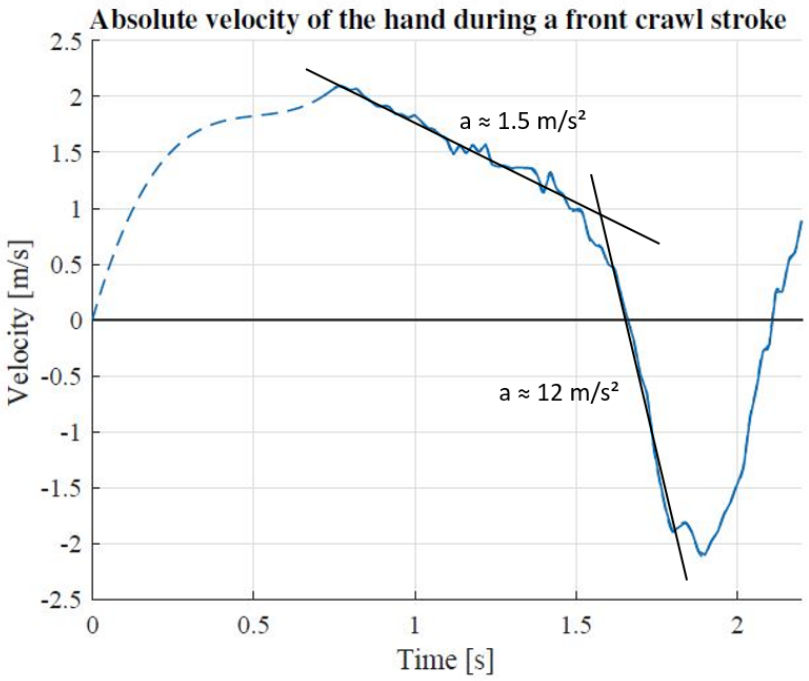

Figure 2 : Velocity of the hand during a front crawl swimming stroke. The start of the propulsion phase is estimated at t = 0.8 s, and the end at around t = 1.8 s, the propulsion phase duration being around 1 s (van Houwelingen et al., 2017b). Note that dashed region corresponds to the recovery phase with interpolated data due to limitation of the camera plan. Reference lines have been added to show estimation of the acceleration a. Figure taken from Bazuin (2018).

1.4. Accelerated plate

In the study of the drag force on an accelerating submerged plate, Grift et al. (2019) performed PIV and force measurements on a flat plate held by a robot arm for simple linear acceleration in an open surface glass tank filled with water. They made multiple experiments for different accelerations toward different plate velocities for three immersion depths of the flat plate. In all cases, they distinguished three phases during the linear motion of the plate: (i) an accelerating phase, (ii) a transition phase, and (iii) a steady phase. Several observations have been made during these different phases via force measurements and flow visualisation and related to hydrodynamic phenomena via PIV measurements. Grift et al. highlighted the formation and dissipation of different shapes of vortices for the three immersion depths, by means of flow visualisation, like a U-shape when the plate is right under the free surface, or a ring-shape for the fully submerged case far from the free surface. With the force measurements, Grift et al. identified the depth generating the maximal drag at stationary state, but they also separated the drag force into its different components: the steady drag force, and the force generated by acceleration of the virtual mass. Particularly, they modelled what they called the residual force F_{mh}, that is the force due to the acceleration of the hydrodynamic mass, second component of the virtual mass after the mass of the plate.

Grift et al. studied the effect of acceleration on an object with a simple geometry, i.e. a flat rectangular plate, and found interesting results in the drag force generated by this plate and the hydrodynamic behaviour of the flow around it for different immersion depths. Here, a similar approach is used in this thesis to study the effect of acceleration on a more complex object, that is a swimmer's hand, for different finger spreading. The experimental set-up is almost identical and similar kinematic conditions are used. Comparisons are done all along this report between the results of both studies.

1.5. Research objectives

The stroke motion in swimming is particularly complex. Several questions remain: the interaction between the arm/hand and the body, the effect of hand configuration in actual swimming motion, drag or lift based stroke motion. Only a few experimental studies on hydrodynamics in swimming combined a realistic stroke motion, where accelerations and decelerations take place, with the complex geometry of the hand. To the knowledge of the author, no study experimentally investigated the effect of acceleration on the different aspects of the hand configuration in the generation of propulsive forces, especially the finger spreading. As a step towards a full comprehension of hydrodynamic propulsion around the hand and the entire body in actual swimming motion and the optimisation of performance, it is necessary to study the combination between unsteady motion and the multiple possibilities of the hand configuration or motion like the finger spreading. In this way, one can wonder: What is the effect of acceleration on the drag propulsion of the hand in swimming, and how does this effect evolve with finger spreading? This thesis will answer that question by performing force and PIV measurements on four 3D printed hands with different finger spreading during simple linear accelerations. Firstly, the effect of acceleration on the drag force generated by a swimmer's hand is investigated for different finger spreading of the hand

and for various kinematic conditions by mean of force measurements. Secondly, PIV measurements are performed to investigate the hydrodynamic phenomena causing the effect of acceleration, combined with the finger spreading of the hand, on the propulsion drag generated by the hand in human swimming.

2. Drag propulsion: acceleration and finger spreading

As showed in section 1.3.3, there are significant variations of the velocity of the hands in swimming strokes, in particular front crawl. It has been argued that accelerations occurring during a swimming stroke enhance propulsive forces by generating unsteady hydrodynamic phenomena (Kudo et al., 2013). Furthermore, as mentioned in section 1.3.1, many studies investigated the effect of finger spreading on propulsion of the hand in swimming and most of them concluded that a small spread between fingers enhances drag (van Houwelingen et al., 2017a). However, all these studies, numerical or experimental, have been done at a stationary state, and none has studied the effect of finger spreading on an accelerating hand.

The objective is to combine the work done by van Houwelingen et al. (2017b) on finger spreading with wind tunnel measurements and by Grift et al. (2019) on an accelerating flat plate with experiments in a water tank. Indeed, a similar experiment as Grift et al. (2019) is performed but now on the 3D printed hands used by van Houwelingen et al. (2017b). In this way, the characteristics of the drag force generated during the acceleration of a swimmer's hand is investigated for different finger spreading. The angle of attack, the thumb position and the cupping have been kept fixed in this study.

This chapter starts by explaining the experimental set-up for the measurement of the drag force on the hands and by presenting the 3D printed hands used and the kinematics of this study. Then, the force signal and the effect of kinematics on this signal are discussed. Finally, the effect of finger spreading on an accelerating hand is presented.

2.1. Experimental set-up

The same experimental set-up as the one used by Grift et al. (2019) for the study of the drag force on an accelerating submerged plate is used in this thesis. It consists of an open square tank made of glass with an edge of 2 m and a height of 0.6 m (Figure 3). The tank is filled with water to a maximum level of 0.5 m to avoid water to spill out of the tank during experiments. 3D printed hands with forearm at full scale used by van Houwelingen et al. (2017b) in wind tunnel experiments that were specially made to investigate the effect of finger spreading on drag of the hand in swimming are used in this study. The hand is mounted on an industrial robot arm (Reis Robotics RL50). A force and torque transducer (ATI 6-DOF), with an acquisition rate of 10 kHz (defined in an automatic acquisition program on Labview), is placed between the robot arm and the 3D hand to measure the forces acting on the hand and arm during the motion. The robot position has an acquisition rate of 92 Hz with a resolution of 1 µm and is repeatable within 0.1 mm (Grift et al., 2019). The angle of attack has been kept fixed at 90°, corresponding to a hand palm perpendicular to the direction of the motion. The immersion depth of the hand has also been kept fixed with a submerged length of hand of 0.4 m, which makes the fingertip at 0.1 m from the tank bottom and the full hand more than 0.2 m deep under the surface. Considering the set-up limitations, this immersion depth has been chosen to be representative of actual swimming conditions during the propulsion phase, where the forearm is fully submerged and perpendicular to the free surface. Bazuin (2018) verified that the flow around the hand and fingers only interacts with one quarter of the forearm, so the

hand is here considered sufficiently deep to assume that there is no interaction between the hand and the free surface. Also, it is assumed that the bottom of the tank is far enough from the fingertip, so it has no effect on the flow around the hand. These assumptions have not been verified in this study. Furthermore, the force due to inertia of the hand and forearm is not negligible. Therefore, some experiments on hands have been done in air to estimate inertia and thus isolate hydrodynamic forces. Due to a lack of repeatability in air measurements, a model for the inertia depending on the acceleration has been created.

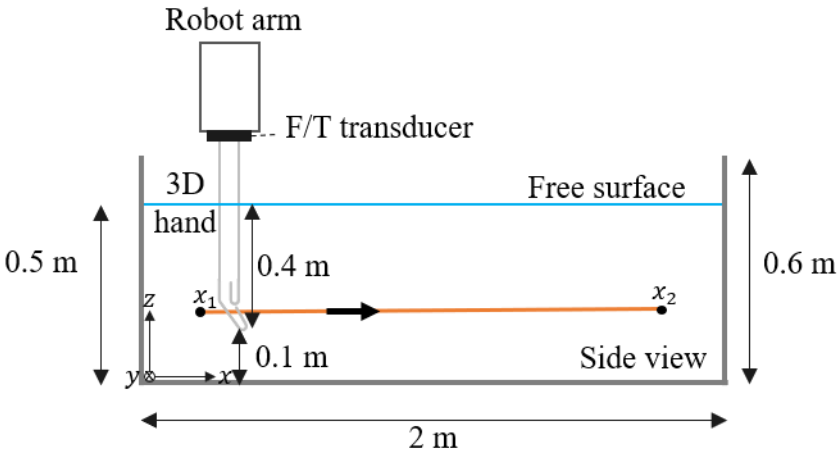

Figure 3 : Side view of the experimental set-up for the force measurements on an accelerating 3D printed hand mounted on a robot arm in a 2 x 2 m water tank, and going from x_1 to x_2.

2.2. Hand models

Four different hand models are here investigated. They were part of the five models that were 3D printed for the study of the effect of finger spreading on drag propulsion by means of wind tunnel experiments (van Houwelingen et al., 2017b). These four hands all have the same neutral cupping, considered as the cupping of a hand at rest, and an identical thumb in an abducted position, so all the hands have the same projected area (van Houwelingen et al., 2017b). They differed in the finger spreading configuration, which are the following: 0° (closed fingers), 5°, 10°, and 20°, as showed in Figure 4. The hand palm width, length and frontal surface (or projected area) of the hands are respectively 0.096 m, 0.507 m and 0.042m². Since the hands are complex objects, the projected area, and the volume of the four hands have been calculated to make sure the force signals of the hands are comparable with each other. Firstly, they have been calculated from the numerical STL files that have been used by van Houwelingen et al., on one hand to implement the models in the simulation and on the other hand to manufacture the 3D printed hands (van Houwelingen et al., 2017b). In the Appendix B.1 are the graphs of the projected area and the volume of the different hands as a function of the submerged length. For the projected area, the curves are very close and partly overlapping, the 20° hand being slightly above and the 0° hand (closed hand) slightly below, the difference in the projected area does not exceed 1%. Secondly, the projected area of the four hands have been directly calculated from pictures of the 3D printed hands to ensure the actual hands have been well manufactured and have not been modified so they perfectly

match the numerical models and all have the same projected area. Figure 5 shows the projected area of the four hands as a function of the hand submerged length but now from the pictures in Appendix B.2. The results are very similar, with again a small difference in the projected area which does not exceed 1%. Moreover, the estimation of the projected area shows a maximum difference of 1.5% between the numerical model and the calculation from pictures of the hands. Therefore, the projected area of the four hands can be considered as equal and the force measurements can be directly used to compare the hands with each other.

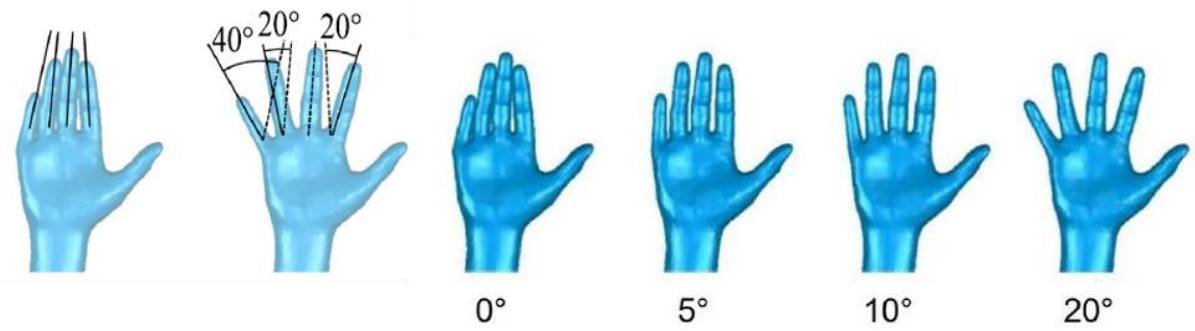

Figure 4 : The four hand models used in this study with hand palm width, length and frontal surface of respectively 0.096 m, 0.507 m and 0.042m². They only differ in the finger spreading, which is respectively 0°, 5°, 10° and 20° (van Houwelingen et al., 2017b).

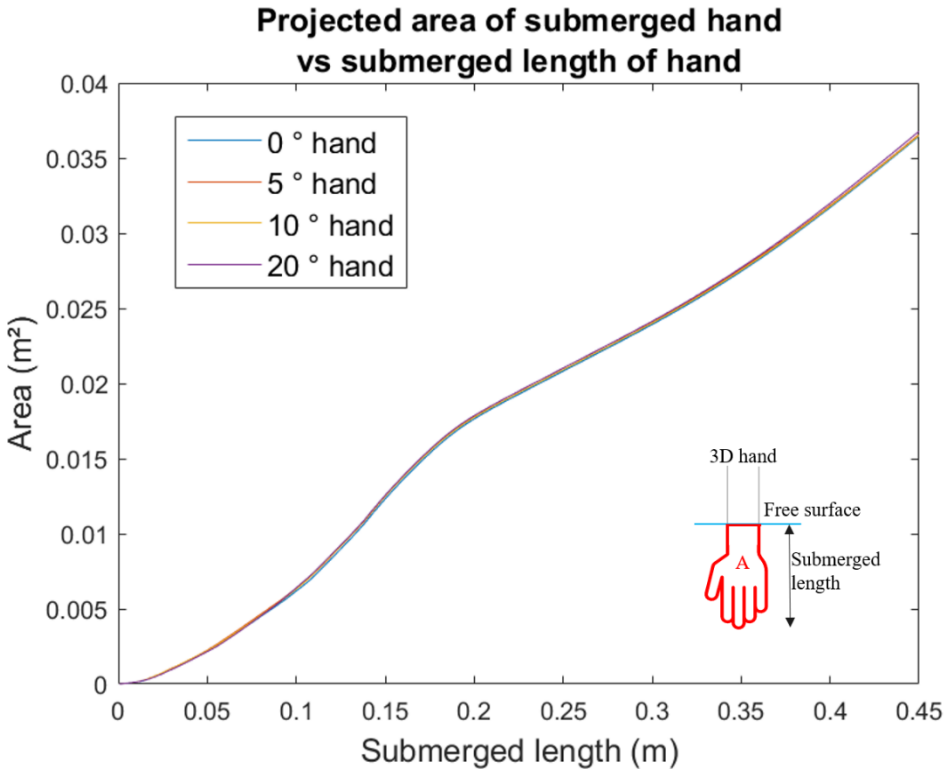

Figure 5 : Projected area of the four hands as a function of the submerged length of hand as described by the scheme on the bottom right of the graph. It has been calculated from pictures of the hands (see Appendix B).

2.3. Kinematics

To investigate the hydrodynamics at stake during unsteady swimming motions and the effect of acceleration on the propulsion drag, a simple linear acceleration has been repeated using the experimental set-up described in the previous section. The studied motion is strictly identical as the one performed by Grift et al. (2019) on an accelerating plate. Figure 6 shows the kinematics of the arm during the motion. The arm initially at rest is accelerated at a given acceleration towards a uniform velocity. Velocities from 0.2 m/s to 0.6 m/s have been reached in the tank with accelerations up to 1.64 m/s², the maximum acceleration the robot arm can perform. Higher velocities, up to 1 m/s, to get closer to actual swimming conditions, have been experimented but the set-up dimensions do not make possible to reach the steady phase at such velocity and so limit the kinematics. As seen on Figure 2 and as mentioned also by Gourgoulis et al. (2010), the velocity of the hand can reach from 2 to 2.5 m/s during the propulsion phase (pull and push phases), three to four times the highest velocity reached in the experiments here. Also, as mentioned in section 1.3.3, accelerations in actual swimming are much higher than the maximum acceleration performed in this study. Section 0 explains why the set-up and the results obtained from these experiments are relevant and representative of actual swimming conditions.

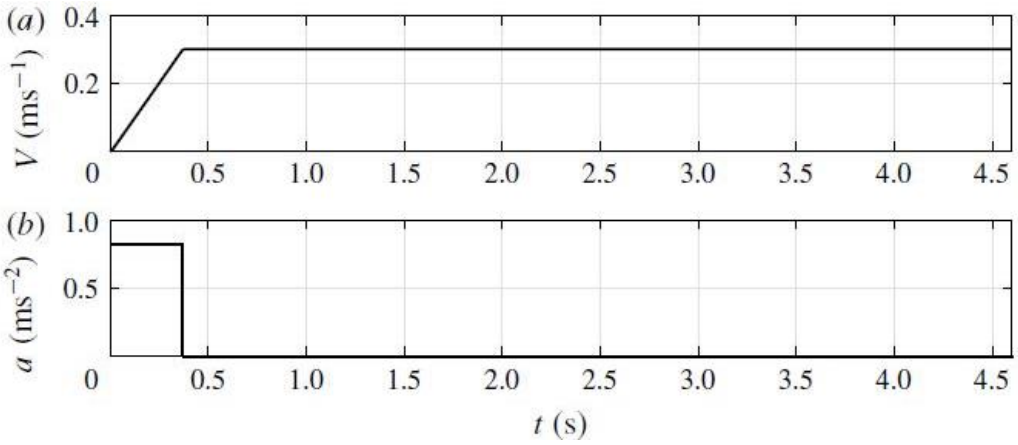

Figure 6 : Arm/hand velocity V and acceleration a (Grift et al., 2019).

The linear acceleration described above has been repeated for different accelerations and final velocities to investigate the effect of acceleration on different finger spreading. For each hand, experiments for four accelerations at a fixed velocity V = 0.6 m/s and for three velocities at a fixed acceleration a = 0.82 m/s² have been done. Table 1 summarises these experiments with force measurements. The experiments have been performed in a random order of velocities and accelerations.

a (m/s²) / V (m/s)	0.42	0.82	1.23	1.64
0.2		x		
0.4		x		
0.6	x	x	x	x

Table 1 : Overview of the set of conditions tested for each hand.

2.4. Force measurements

2.4.1. Force signal

The procedure is very similar to the one used by Grift et al. (2019). During each experiment, the instantaneous force is recorded and sampled at a 10 kHz rate via an acquisition program on Labview. Figure 7 shows a typical force signal as a function of time for an experiment with an acceleration a = 0.82 m/s² and velocity V = 0.4 m/s on a hand with a finger spreading of 5°. The corresponding graph of the velocity as a function of time appears below the first graph. The original signal is particularly noisy, that is why the signal is filtered with a second order Savitzky-Golay filter with a 0.1 window corresponding to 1001 samples. This filter succesively finds for each point the second order polynomial that fits the signal within the given window by minimizing the least squares error. When dealing with an accelerating object, the drag force must contain the effect of added mass, and is defined as a function of time as follow (Grift et al., 2019):

$$\boldsymbol{F_d(t) = F_{C_d}(t) + F_{vm}(t) = \frac{1}{2}\rho_f V(t)^2 C_d A + (m_{hn} + m_{hd})\, a(t)} \quad (2)$$

Where F_{C_d} is the corresponding steady drag force at an instantaneous velocity $V(t)$ and F_{vm} is the force due to virtual mass generated by acceleration. F_{C_d} corresponds to the traditional drag force in a steady flow described in (1). F_{vm} is the product of the imposed acceleration and the virtual mass, which is composed by the hand mass m_{hn} and the hydrodynamic mass m_{hd} (Grift et al., 2019). The hydrodynamic mass m_{hd} multiplied by the acceleration corresponds to the residual force F_{mh} (Grift et al., 2019).

The three phases distinguished by Grift et al. (2019) are observed here. The end of the acceleration at around t = 0.5 s matches with the initial peak observed in the force signal, called the acceleration peak, due to the added mass generated by the acceleration. This first phase between the start at t = 0 s and the acceleration peak corresponds to the acceleration phase identified as A in Figure 7. After the peak, the force signal decreases during the transition phase (B) until around t = 3 s to reach a stationary state and the final phase called the steady phase (C) where the force becomes constant and equal to the steady drag force F_{C_d}. At the very beginning of the signal, a local peak is observed and has been identified by Grift et al. as a step response caused by the flat plate stiffness which would be the hand stiffness here (Grift et al., 2019). A length of 400 mm of hand is submerged. For the deeply submerged plate, Grift et al. identified large flow structures in the wake of the plate resulting in peaks in the force signal during the transition phase, these peaks are not observed here. However, a small “plateau” is observed just after the acceleration peak, the hydrodynamics will be investigated using PIV.

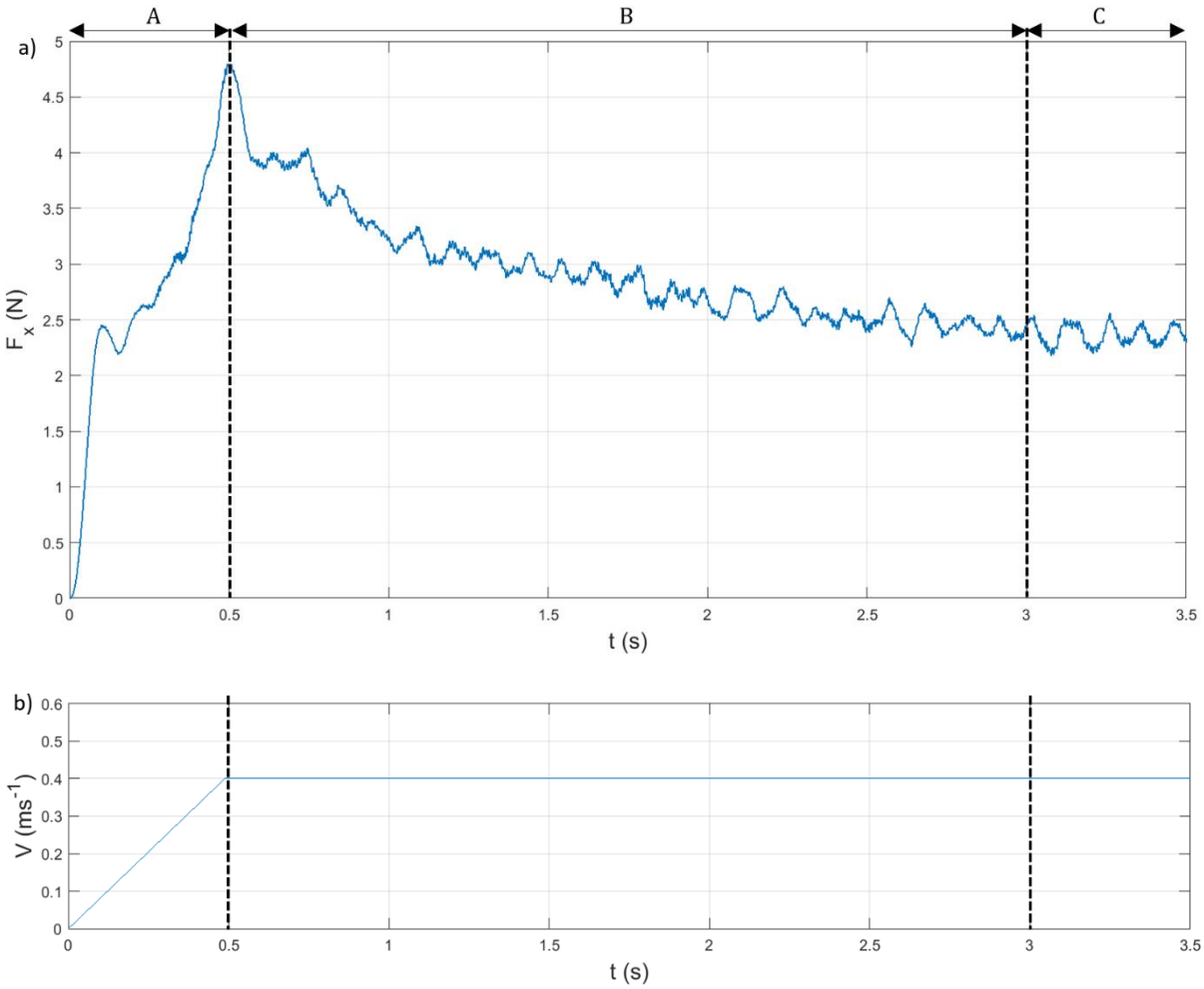

Figure 7 : a) Typical force signal with three distinct phases (A, B and C) respectively the acceleration phase, the transition phase and the steady phase. b) The hand velocity as a function of time corresponding to the force signal with an acceleration a = 0.82m/s² and a velocity V = 0.4m/s.

2.4.2. Repeatability

To check on the repeatability of the experiment and the force measurements, each set of conditions (acceleration and final velocity) has been repeated at least three times. To illustrate the repeatability, Figure 8 shows the results of the repeated experiments for two hands with opposite finger spreading: the closed hand (a) and the 20° finger spreading hand (b) which corresponds to the maximum spread investigated. The graphs on the left represent three identical trials, the ones on the right show the mean force signal with the standard deviation (dashed signals). The force measurements are highly repeatable for both hands. During the acceleration phase, the trials are very close and partly on top of each other.

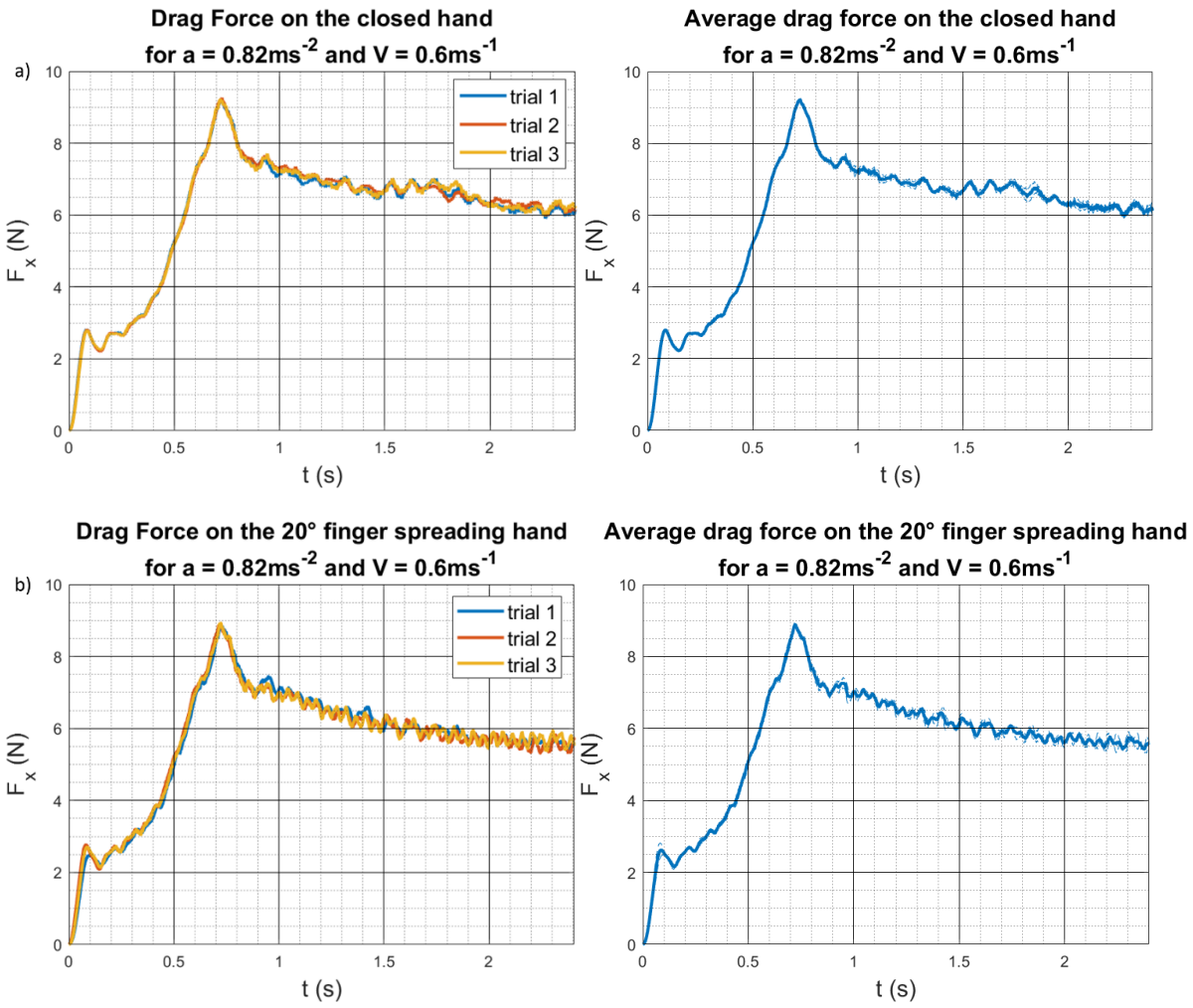

Figure 8 : Repeatability of the force measurements for two hands at a = 0.82ms^{-2} and V = 0.6ms^{-1}. a) The closed hand and b) the 20° finger spreading hand. Each experiment is repeated three times. The left graph shows drag force as a function of time for the three trials, the right graph shows the average drag force as a function of time with the corresponding standard deviation (dashed signal).

After the acceleration peak, during the transition phase and the steady phase, the signals are oscillating but still show a good repeatability with a maximum standard deviation in the data of 3%. The Appendix A contains other graphs showing the repeatability of the force measurements including different hands and set of conditions.

2.5 Effect of kinematics

2.5.1. Force signal: acceleration and velocity

As explained in 2.3, the linear acceleration has been performed for various set of acceleration and velocity on the different hands. Figure 9 shows the effect of variation of the kinematics on the drag force as a function of time. On one hand, the force signal of the closed hand for

different accelerations with a final velocity V = 0.6 m/s and on the other hand, the drag force on the 20° finger spreading hand for various final velocities with an acceleration a = 0.82 m/s². Similar effects as for the accelerating plate are observed (Grift et al., 2019). One can see on the first graph that the acceleration peak due to added mass scales with the acceleration as expected from (1), with a peak 25% larger for the highest acceleration compared to the lowest. However, the steady phase does not depend on the acceleration, the curves all converge the same way. As mentioned by Grift et al. for the plate, here also the steady phase drag force scales with V² as expected from (1) whereas during the acceleration phase, the drag force linearly increases with time and therefore scales with V which is not expected from (1). As showed by the second graph, the acceleration phase does not depend on the final velocity. Indeed, the curves are perfectly overlapping before to successively reach the initial peak. The graphs are representative of the effect of variation of kinematics on the drag force for all the hands.

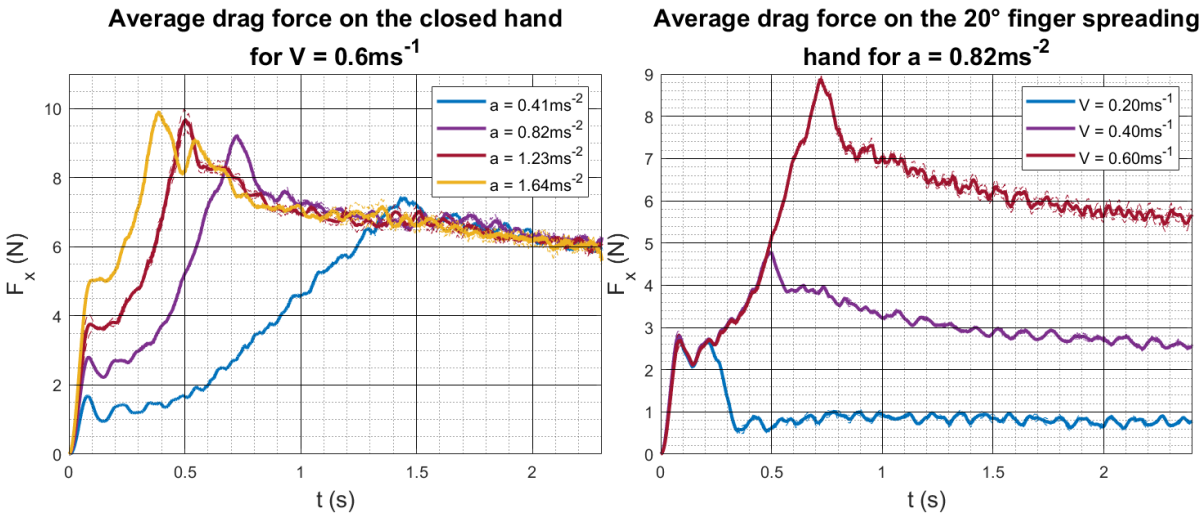

Figure 9 : Average drag force as a function of time on the closed hand for different accelerations with V = 0.6 m/s on the left graph, and on the 20° finger spreading hand for different velocities with a = 0.82 m/s² on the right graph.

2.5.2. Reynolds dependency

The Reynolds number is the ratio of the inertial forces and the viscous forces and is defined as:

$$Re = \frac{D\,V}{\nu} \tag{3}$$

Where V is the flow velocity with respect to the object, D is the characteristic length of the object and ν is the kinematic viscosity of the fluid. Re is often used for scaling to make dynamic similarity for experiments performed in different conditions and can be used here. Since the 3D printed hands are full scale and the experiments are performed in water (at 20°C), the velocity of the robot arm would need to be equal to swimming hand velocity to perform the experiments in the same range of Re as actual swimming conditions. However, as

mentioned in section 2.3, the velocity reached in the experiments are four times lower than in actual conditions. The characteristic length D is the hand palm taken as 0.1 m, so the range of Re investigated in this study is from 2 x 10^4 to 6 x 10^4 whereas the range goes up to around 4 x 10^5 for the hand in human swimming.

Van Houwelingen et al. (2017a) showed from many numerical studies on the drag around a swimmer's hand that none of them found a clear dependence of C_d on velocity for Re between 2 x 10^4 and 4 x 10^5, only one experimental study found significant changes for velocities lower than 5 m/s. Bazuin (2018) compared the drag coefficient obtained for a circular cylinder and full scale hands for Re between 2 x 10^4 and 1.8 x 10^5. He found small changes in C_d with the velocity but concluded that these were due to a surface piercing effect only so that the drag coefficient of a hand model is intrinsically independent on the Reynolds number at the given range.

The drag coefficient C_d has been calculated here, for different velocities from the steady phase mean drag force F_{C_d} at constant velocity. Figure 10 shows the results for two hands with different finger spreading, for target velocities from 0.2 m/s to 0.6 m/s corresponding to the range of Re mentioned before, with an acceleration a = 0.82 m/s² . The error bars correspond to the standard deviation of C_d for at least three repetitions. Non negligeable differences can be observed in the mean values of C_d for the different velocities. However, considering the standard deviation of the data, the ranges are partly overlapping. So, regarding these results and the conclusion made in different studies, especially by Bazuin (2018), it is assumed that the drag is independent of velocity in the range of Re investigated and therefore, the results generated in this study will be considered representative for actual swimming conditions.

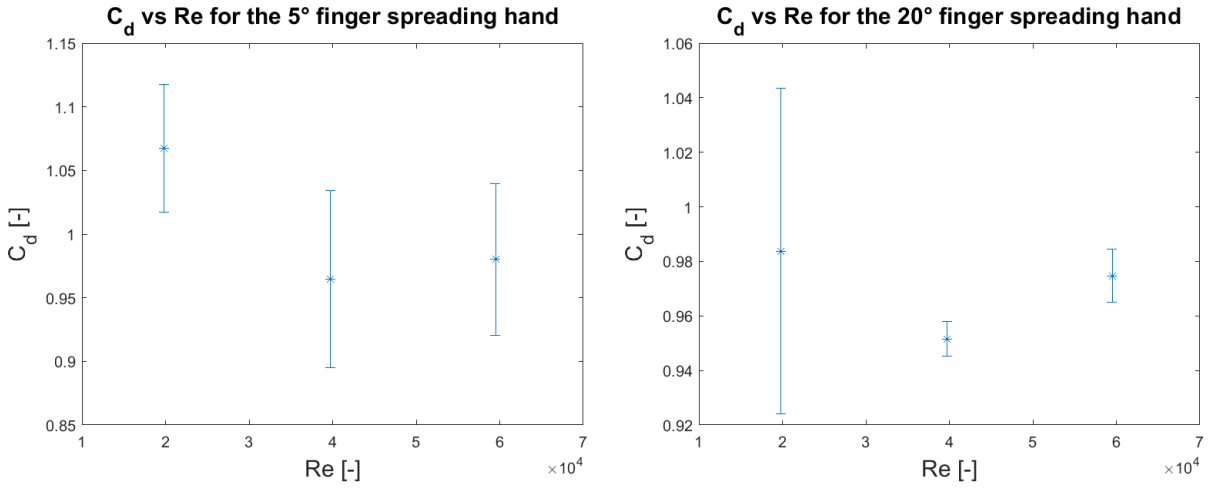

Figure 10 : Graphs of the drag coefficient C_d, calculated from the mean drag force during the steady phase, as a function of the Reynolds number Re , for the 5° finger spreading hand on the left and the 20° finger spreading hand on the right. Note that the results are from separated set of experiments done with slightly different immersion depths (results on the 5° hand are from an early set of experiments done at a 0.39 m submerged length of hand, while the results on the 20° hand have been done with a 0.4 m submerged length like the rest of the experiments).

2.6. Finger spreading effect on the drag for accelerating hands

2.6.1. Force signals for selected kinematic conditions

Three sets of kinematic conditions have been selected to compare the different finger spreading in the force measurements: a = 0.82 m/s² with V = 0.4 m/s and V = 0.6 m/s and a = 1.64 m/s² with V = 0.6 m/s. In Figure 11 are the three graphs corresponding to the three sets of conditions. They show the drag force F_x of each hand as a function of time. Very small differences are observed during the acceleration phase for the three sets, the force signals are close to each other and mostly within the respective standard deviations. There are small differences in the acceleration peak that will be discussed. During the transition phase an increasing gap between the closed hand (0°) and the other hands can be observed in the three cases. This gap reaches a maximum around the middle of the transition phase. It slightly decreases during the end of the transition phase and finally stabilises during the steady phase.

At a = 0.82 m/s² and V = 0.4 m/s (Figure 11 a), the acceleration peaks at 0.5 s are very close to each other, the 0° hand has the highest peak with 4.83 N but less than 1.5% bigger than the lowest peak, which is in the standard deviation range. At the beginning of the transition phase, at around 0.6 s, the force signal of the closed hand starts to differ where the drag force becomes higher than for the other hands and this gap is slowly increasing during the transition phase. While the force signals of the 5°, 10° and 20° hands are continuously decreasing during that phase, the force signal of the 0° hand seems to stabilise between 1.8 s and 2.2 s despite the oscillations, which makes the gap with the other hands bigger than 10% at 2.1 s. At the steady phase, the 0° hand drag force is higher by more than 6% than the 20° hand, which has the 2nd highest steady drag force by less than 2% compared to the other two hands. Finally, the total drag force after the acceleration peak has been computed by calculating the area under the curve using trapezoidal integration, and is at least 6% higher for the closed hand compared to the others. The difference between the three hands with finger spreading (5°, 10°, 20°) is below 1.3% which is not significant considering the standard deviation of the data.

At a = 0.82 m/s² and V = 0.6 m/s (Figure 11 b), the observations are very similar except for the initial peak. A more significant difference appears at the acceleration peak (t = 0.73 s) with a 3.5% difference in force between the two extremes (the closed hand has the highest force, the 20° hand the lowest), the standard deviation being under 1.5% at the peak for the four hands. During the transition phase, the increasing gap between the closed hand and the other hands is observed with a maximum above 10% at t = 1.7 s. The steady drag force of the 0° hand (6.28 N) is 8% higher than the other three. Finally, the total drag force after the initial peak is 5.5% to 7% higher for the closed hand.

For the third set of kinematic conditions at a = 1.64 m/s² and V = 0.6 m/s (Figure 11 c), the observations are again similar except for the initial peak. A difference of 3% is observed in the force peak (t = 0.38 s) but this time the closed hand has the lowest peak value, and the 5° hand has the highest. During the transition phase, the drag force of the closed hand becomes again greater than for the hands with a finger spreading. The gap between the closed hand and the three others can be observed and it reaches more than 9% at t = 1.35 s. The steady drag force of the closed hand (6.24N) is at least 6.5% higher than the other three and the area under the curve after the initial peak is from 4.3% to 6.6% greater for the closed hand.

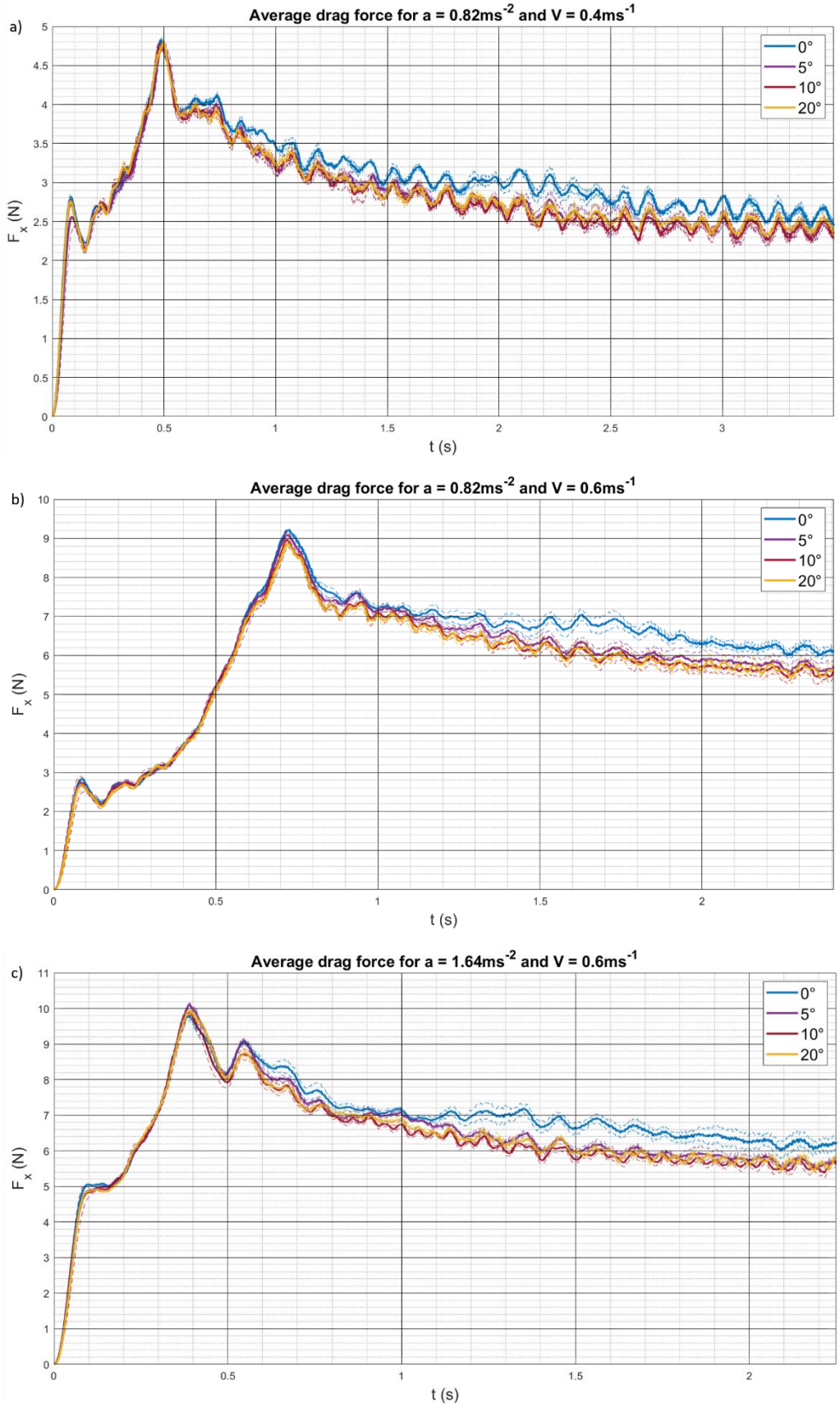

Figure 11 : Average drag force of the four hands with different finger spreading (0° for the closed hand, 5°, 10° and 20°) as a function of time for 3 set of conditions : a) a = 0.82m/s² and V = 0.4m/s, b) a = 0.82m/s² and V = 0.6m/s and c) a = 1.64m/s² and V = 0.6m/s.

The force signals for the kinematic conditions selected clearly show a higher drag force for the closed hand compared to hands with finger spreading. The difference appears during the transition phase while no significant difference is observed during the acceleration phase. The 10° finger spreading hand seems to be the least efficient in terms of drag generated but the difference with the 5° and 20° finger spreading hands are small and within the standard deviations of the signals.

2.6.2. Effect of finger spreading on the steady phase drag

During the steady phase, the force signal is equal to the steady drag force F_{C_d} at constant velocity and the drag coefficient C_d can be calculated as in section 2.5.2. Figure 12 shows the drag coefficient, calculated from the mean drag force during the steady phase, as a function of the finger spreading of the hand for measurements at V = 0.6 m/s and two different accelerations: a = 0.82 m/s² and a = 1.64m/s². First, as mentioned in section 2.5.1, it can be noticed that the drag coefficient is not dependant on the acceleration. Indeed, for each finger spreading, the difference in C_d between the two accelerations is small (below 1% between mean values) and can be considered negligeable taking into account the respective standard deviations. Secondly, as seen in the previous section 2.6.1, the closed hand has a higher drag

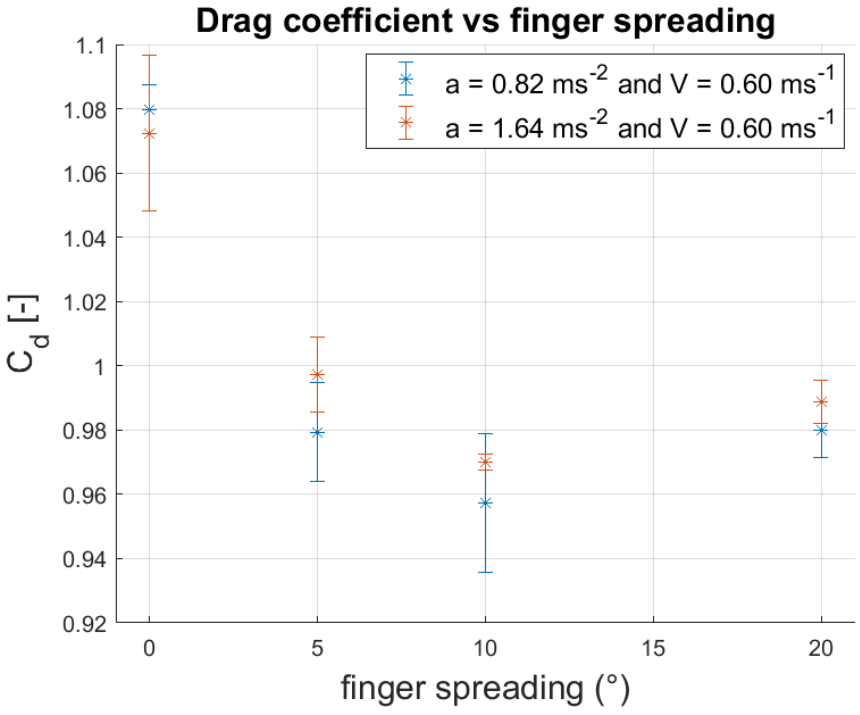

Figure 12 : Drag coefficient calculated from the mean drag force during the steady phase of the force signal, for two different accelerations with a target velocity V = 0.6 m/s, as a function of the finger spreading (closed hand and 5°, 10° and 20° finger spreading). Note that the result on the 5° hand for a = 0.82 m/s² differs from Figure 10 since it comes from a different set of experiments as explained before.

coefficient C_d than the three other hands with finger spreading, with an increase of approximately 7% compared to the 5° finger spreading hand and 9% compared to the 10° finger spreading hand. This result on the drag dependency on the finger spreading does not agree with the literature, particularly with van Houwelingen et al. (2017b) who found an optimal drag coefficient for the 5° finger spreading via wind tunnel measurements on the same models while they found optima at 10° and 20° via numerical simulation (van Houwelingen et al., 2017b). For the closed hand, van Houwelingen et al. found an experimental value for the drag coefficient of 1.12 against 1.08 here. However, the differences are much larger for the hands with finger spreading (C_d = 1.14 for the 5° hand against around 0.99 here).

2.7. Conclusion

The typical force signal is very similar as for the accelerated plate (Grift et al., 2019). A step response due to the hand's stiffness, a peak which coincide with the end of the acceleration and three distinct phases are observed: an acceleration phase ending with a peak due to virtual mass, followed by a transition phase where the force gradually decreases leading to a constant value during the steady phase corresponding to the steady drag force. Furthermore, the force measurements are highly repeatable with a maximum standard deviation of the data < 3% all along the force signal.

The effect of the variation of kinematics on the drag force are very similar as for the accelerating flat plate (Grift et al., 2019). The drag force during the acceleration phase scales with V but does not depend on the target velocity for a given acceleration. The acceleration peak due to added mass scales with the acceleration a. During the steady phase, the drag force scales with V^2. Moreover, from different studies, it seems that the drag coefficient has no dependence on velocity in the range of Reynolds number investigated which ensure the results and conclusions of this study to be representative of actual swimming conditions. However, it would be interesting to perform experiments on hands, in absence of a free surface, for $1 \times 10^4 \leq Re \leq 5 \times 10^5$, from the low velocities performed in the experiments of this study to realistic swimming velocities, to precisely evaluate C_d as a function of the velocity only avoiding the possible effect of the free surface on C_d, as mentioned by Bazuin (2018).

The comparison of the different finger spreading showed a net advantage for the closed hand in the drag force generated during the motion experimented. Similar observations were made for the three set of kinematic conditions presented. The difference starts to grow right after the acceleration peak and becomes significant during the transition phase and finally stabilizes during the steady phase, leading to a higher drag force, and consequently a higher power generated, all over the motion by the closed hand compared to the hands with a finger spreading (5°, 10° and 20°). Consequently, a closed hand leads to a significant increase in the drag coefficient C_d, calculated from the steady phase drag force, compared to the three other hands. This result does not agree with most of the literature which found that, for steady motion, a small finger spreading induces higher propulsive forces (van Houwelingen et al., 2017b). That shows that acceleration is key when investigating the effect of hand configuration on propulsive forces. The divergence between the results on the steady drag

force in this study and the results for steady motion in the literature might be due to an effect of the acceleration still existing during the steady phase. Visualisation of the flow dynamics using PIV will enable a better understanding of these results.

3. Hydrodynamics around accelerating hands

Several observations have been done on the drag force measurements including a force peak at the end of the acceleration, scaling with the acceleration, but also a higher drag generated by the closed hand, especially during the transition phase. One can wonder what hydrodynamic phenomena are causing these observations. PIV enables the visualisation of these phenomena.

First, this chapter describes the PIV experimental set-up before to present the different PIV and processing parameters chosen. Finally, the results are discussed, including the repeatability of the flow dynamics and the observations of the unsteady phenomena for the four hands with different finger spreading, at various accelerations.

3.2. Experimental set-up

A planar PIV set-up similar to Grift et al. (2019) set-up has been implemented in the water-filled glass tank (Figure 13).

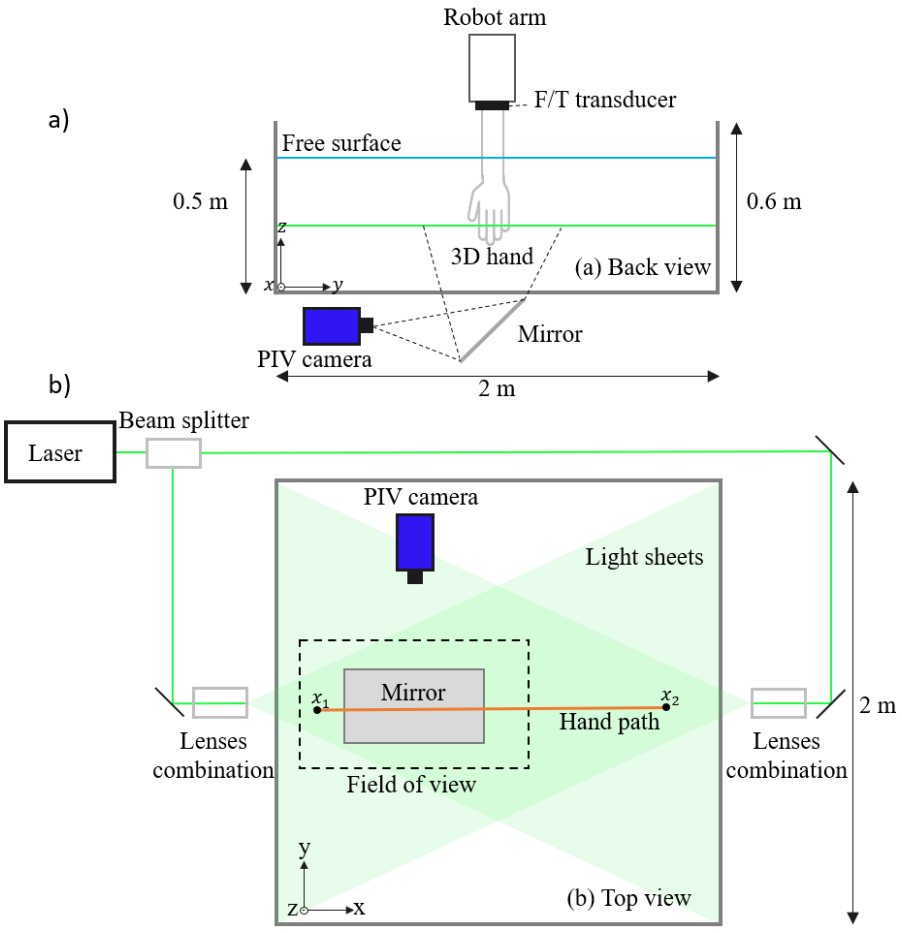

Figure 13 : Scheme of the experimental set-up including PIV measurements system. a) Back view of the set-up with the robot arm holding the 3D printed hand and the high-speed camera underneath the tank recording the hand motion for PIV. b) Top view with the laser beam, split to create two opposite light sheets using a combination of mirrors and lenses, the linear hand path from point 1 (x_1) to point 2 (x_2) and the PIV camera field of view.

PIV is used to capture and investigate the hydrodynamic phenomena around the hand caused by acceleration for different finger spreading. The PIV experimental set-up measure the displacement of fluorescent spherical particles added to the water. The light source to illuminate the particles is a laser beam which is first split in two separate beams. Then, these two beams are directed on the opposite sides of the glass tank in the hand's motion direction using mirrors. After, for both beams, spherical lenses are combined with a cylindrical lens to create two overlapping laser sheets and so avoid shadow from the hand on the light sheet. Underneath the tank, a high-speed camera is used to record the experiment and capture the particles displacement. To increase the field of view, the camera is placed parallel to the motion pointing at a 45° mirror. The camera and the mirror are positioned to capture the first half of the motion, containing the acceleration phase, and a part of the transition phase.

3.3. PIV parameters

As explained above, the field of view of the high-speed camera has been broadened to capture a bigger part of the hand motion, using a 45° mirror with the camera placed under the tank pointing at the mirror. A double pulse laser has been used and configured to generate a single pulse laser beam by synchronising the two pulses. The time between two images is therefore defined by the frame rate of the camera, which is also equal to the pulse rate of the laser. The recording time, the acquisition rate, and the field of view of the system are limited by the camera's memory. To have a high acquisition rate, keeping a sufficient recording time to capture the full motion, the field of view is cropped in the y direction, perpendicular to the hand motion, far enough from the hand where the flow is not disturb during the motion (Figure 14). So, the dimensions of the field of view are 777 x 357 mm.

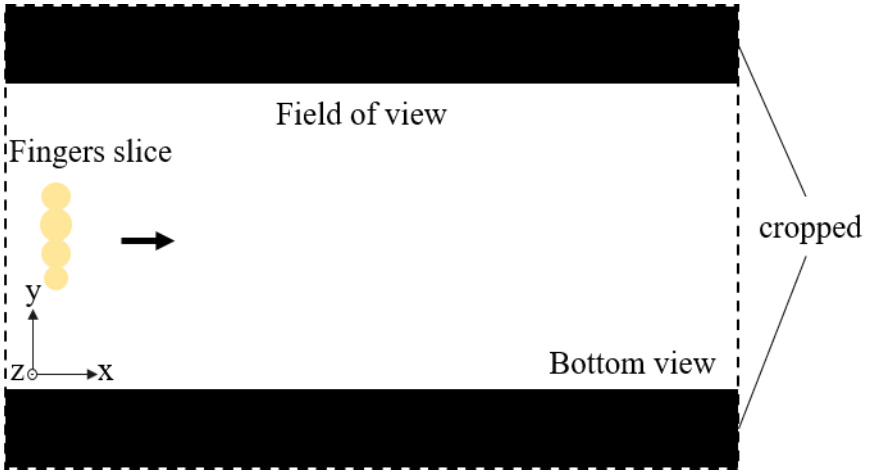

Figure 14 : Schematic of the field of view on the high-speed camera. The initial field of view is cropped in the y direction to reach a higher acquisition rate.

Table 2 gives an overview of the main parameters of the PIV set-up and post processing. The laser sheet is positioned at around 70 mm from the fingertip, slightly under the first phalange (from hand palm) of the middle finger as showed in Figure 15, far enough from the hand palm to focus on the flow behaviour around the fingers but close enough so the plan always crosses

the four fingers. The hands being complex objects, out-of-plane motion can be expected around the hand and the fingers, this can alter correlation since it can cause particles images to change intensity or particles to disappear and new ones to appear in the light sheet, knowing that only particles that appear in both images of an image pair contribute to the displacement peak in the correlation plane (Keane & Adrian, 1992; Scharnowski & Kähler, 2020). Keane and Adrian (1992) proposed that the out-of-plane displacement should not exceed one quarter of the light sheet thickness, known as the 'one-quarter-rule'. Therefore, the thickness of the light sheet, approximately determined using a ruler, has been taken as 3 ± 1 mm, large enough to ensure good correlation. A minimum particle density d_p of 8.58 x 10^4 particles/m² has been chosen to have a mean of 8 particles per interrogation window. Since sedimentation occurs on the particles, the water is mixed before each PIV experiment to get a homogeneous distribution of the particles in the tank, so the minimum particle density is ensured. A maximum acquisition rate has been fixed at 1.3 kHz so an optimal time increment can be chosen for the post processing of the images pairs. A three images increment corresponding to 2.31 ms has been taken for the calculation of the velocity field, to have a particle displacement large enough between two images while having a limited out-of-plan motion of the particles, so the 'one-quarter-rule' is respected and loss-of-correlation is limited.

Field of view (x x y)	777 x 357 mm (2583 x 1188 px)
Laser sheet thickness	3 ± 1 mm
Recording	Single frame, single exposure
Initial PIV interrogation window	64 x 64 px (1 pass)
Final PIV interrogation window	32 x 32 px (3 passes)
Vector spacing	16 px (50% overlapping)
Calibration (pixel/mm)	3.314 px/mm
Particle diameter D_p	53-63 µm
Particle density d_p	≥ 8 p/window = 8.58 x 10^4 p/m²
Camera acquisition rate	1.3 kHz
Exposure time delay	2.31 ms (3 images increment)

Table 2*:* Parameters of the PIV set-up and post-treatment.

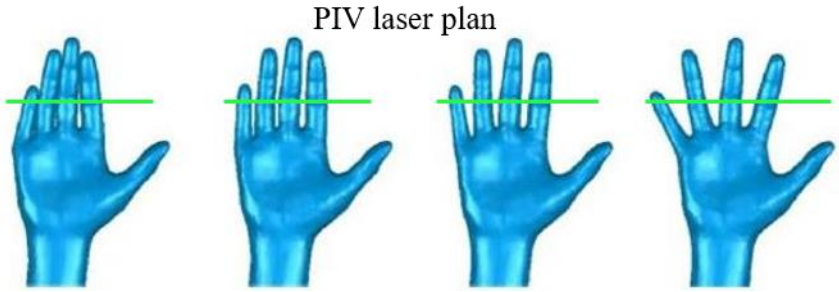

Figure 15 : Position of the PIV laser plan (in green) for the four hands investigated.

3.4. Results and discussion

3.4.1. Repeatability

The flow in the wake of the hands for the different kinematic conditions becomes quickly turbulent, with the generation of vortices starting from the finger edges and dissipating in the wake as illustrated Figure 16, which shows the vorticity field around the 5° finger spreading hand at the middle of the transition phase (t = 1.5 s) for a = 0.82 m/s² and V = 0.6 m/s.

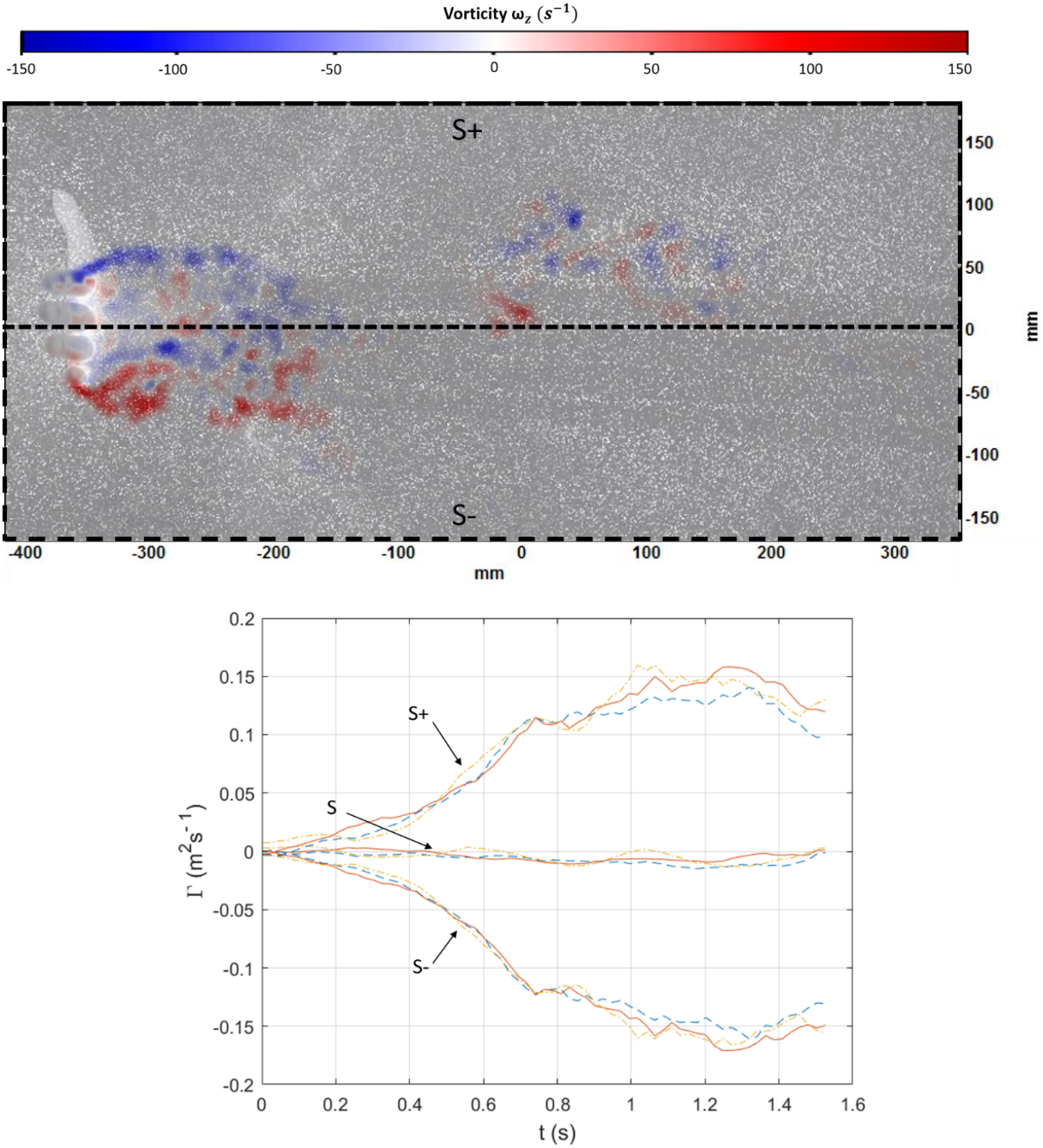

Figure 16 : Vorticity ω_z at t = 1.5 s around the 5° finger spreading hand for a = 0.82 m/s² and V = 0.6 m/s. Below, the corresponding circulation Γ as a function of time between t = 0 s and t = 1.5 s, computed around the 5° hand for three trials (different colours) and three surfaces: the total flow field S divided in the top-half and bottom-half surfaces S+ and S-.

As Grift et al. (2019), the circulation Γ around the hand has been computed as a function of time to quantify the hydrodynamic phenomena around the hand. Figure 16 shows the computed circulation based on the total flow field S, the top-half surface S+ and the bottom-half surface S-, for three realisations. Despite small deviations can be noticed, the highly turbulent flow dynamics seem well repeatable regarding the circulation, as Grift et al. (2019) showed for the flat plate. Also, the computed circulations respectively based on S+ and S- show very similar variations, so only the top-half surface S+ is considered in the rest of this study when comparing circulation, and the circulation corresponding to S+ is denoted Γ+. Appendix C.1. shows the computed circulation for realisations around the 20° finger spreading hand with captures of the vorticity field at t = 1.5 s.

3.4.2. Effect of acceleration

The force measurements showed that the acceleration peak due to virtual mass in the drag force signal, observed at the end of the acceleration, scales with the acceleration as it could be expected. Flow visualisation enables to observe how it is translated in terms of hydrodynamics of the flow. Figure 17 (a) shows the vorticity fields for three different accelerations, with a target velocity V = 0.6 m/s, at times close to the respective ends of acceleration phase: 1.4 s for a = 0.41 m/s², 0.7 s for a = 0.82 m/s and 0.35 s for a = 1.64 m/s². One can see that a pair of vortices is created at both sides of the four fingers of the hand as it has been mentioned by Grift et al. (2019) for the flat plate. It can be noticed that the higher the acceleration is, the stronger and the more concentrated the vortices are. Indeed, for the case a = 1.62 m/s², the pair of vortices stays very close to the hand at the end of the acceleration while for the case a = 0.41 m/s², the vortices start to dissipate and move away from the hand, so the wake behind the hand is three to four times longer compared to the first case mentioned. The circulation Γ+ based on the top-half surface S+ (Figure 16) has been computed at the respective times mentioned above, and the higher the acceleration, the lower the total amount of circulation is. Indeed, Γ+ is more than 30% larger for the case a = 0.41 m/s² compared to a = 1.62 m/s². However, the wake being much shorter for the highest acceleration, the amount of circulation is larger close the hand than for the lowest acceleration, so a lower pressure can be expected right behind the hand resulting in a larger drag force. This can explain that the acceleration peak generated in the drag force scales with the acceleration (Figure 17 b).

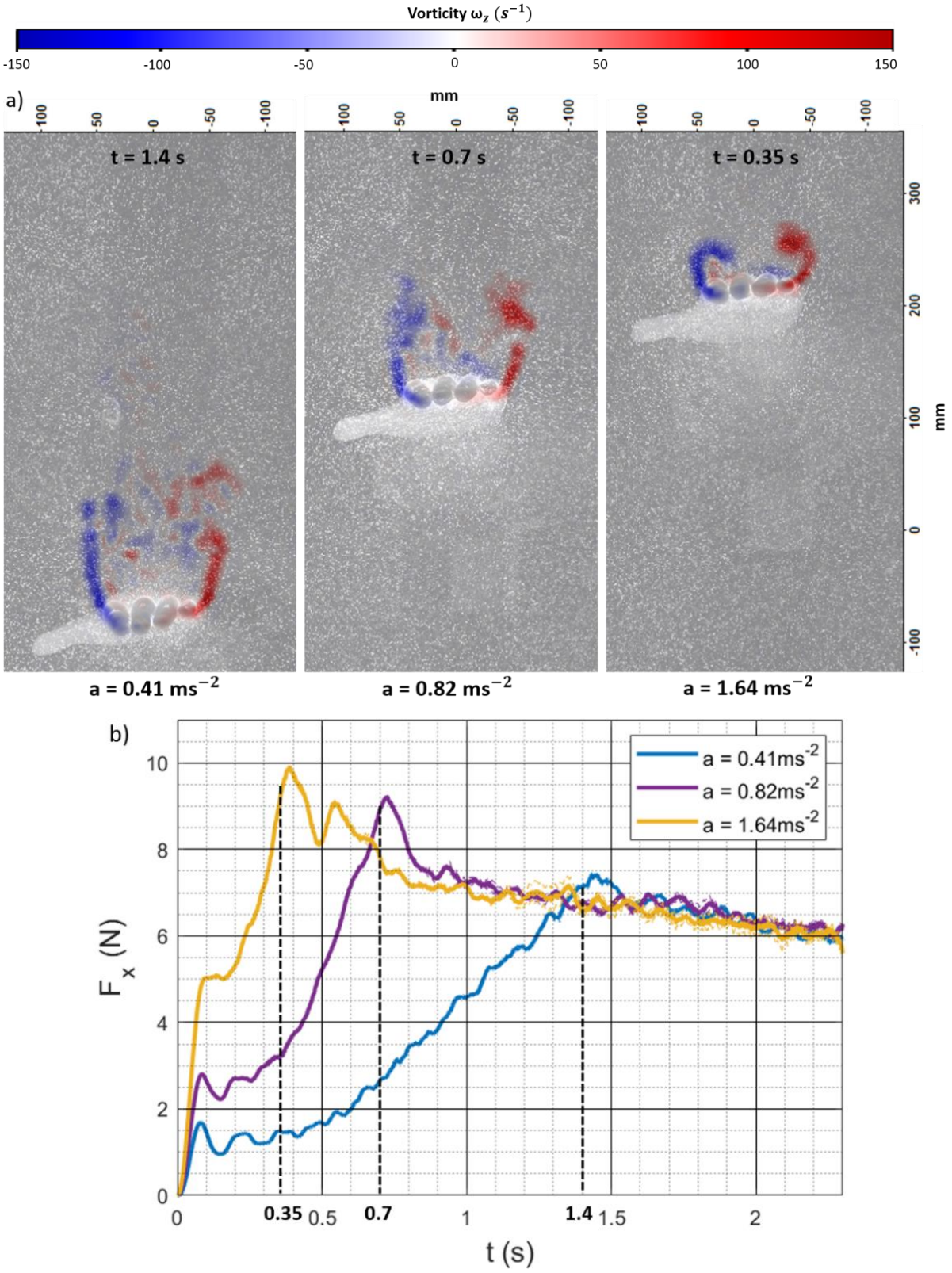

Figure 17 : a) Vorticity ω_z of the closed hand for three different accelerations with a target velocity V = 0.6 m/s close to the respective end of acceleration times with b) the corresponding average drag force as a function of time (as in Figure 9).

3.4.3. Effect of finger spreading

The drag force measurements on the four hands with different finger spreading presented in section 2.6 showed very similar results for the various kinematics conditions investigated. That is why, only one set of acceleration and target velocity has been investigated in detail for the comparison of the flow fields around the four hands using PIV. The results for an acceleration a = 0.82 m/s² with the highest velocity tested V = 0.6 m/s are discussed. The corresponding force measurements are shown in Figure 11 (b). Figure 18 shows the vorticity ω_z in the selected plan (Figure 15) for the four hands at three different times, t = 0.7 s, t = 1 s and t = 1.5, respectively corresponding to the end of the acceleration, the beginning and the middle of the transition phase. At t = 0.7 s, the closed hand and the 5° and 10° finger spreading hands show a pair of vortices as mentioned previously, also observed by Grift et al. (2019) for the flat plate. The vortices seem to be slightly more dissipated for the 5° and the 10° hands compared to the closed hand and break earlier on the little finger side. Indeed, the closed hand and the 5° hand have a top-half circulation Γ+ from 5% to 10% larger than the 10° hand, while the amount of circulation around the closed hand is larger close to the hand compared to the 5° hand. For the 20° hand, the wake is already chaotic due to jets between the fingers, these jets do not appear for the 5° and 10° hands probably due to a blockage effect of boundary layers around the fingers (van Houwelingen et al., 2017a). At t = 1 s, Γ+ is 3% to 14% larger for hands with finger spreading compared to the closed hand. However, the bigger the finger spreading (10° and 20°), the further the vortices are travelling away from the hand which make the amount of circulation higher close to the hand for the closed hand, and might cause the quicker decrease of the drag force for the hands with finger spreading during the transition phase. At t = 1.5 s, the wake is highly chaotic for the 20° hand, while the vortices for the 10° hand are less concentrated and move far away from the hand compared to the closed hand and the 5° hand. The circulation Γ+ is 25% larger for the closed hand compared to the 5° hand, which could explain, combined with to the different lengths of hand's wake, the higher drag force generated by closed hand during the transition phase compared to the three others. Appendix C.2 shows the circulation Γ based on the entire flow field S, and on the half surfaces S+ and S-for the four hands as a function of time.

Additional PIV experiments have been done to capture the second half of the motion by moving the camera and the mirror (Figure 19), and observe the flow hydrodynamics for the different finger spreading during the second half of the transition phase and during the steady phase. The fields of view are overlapping by around 100 mm.

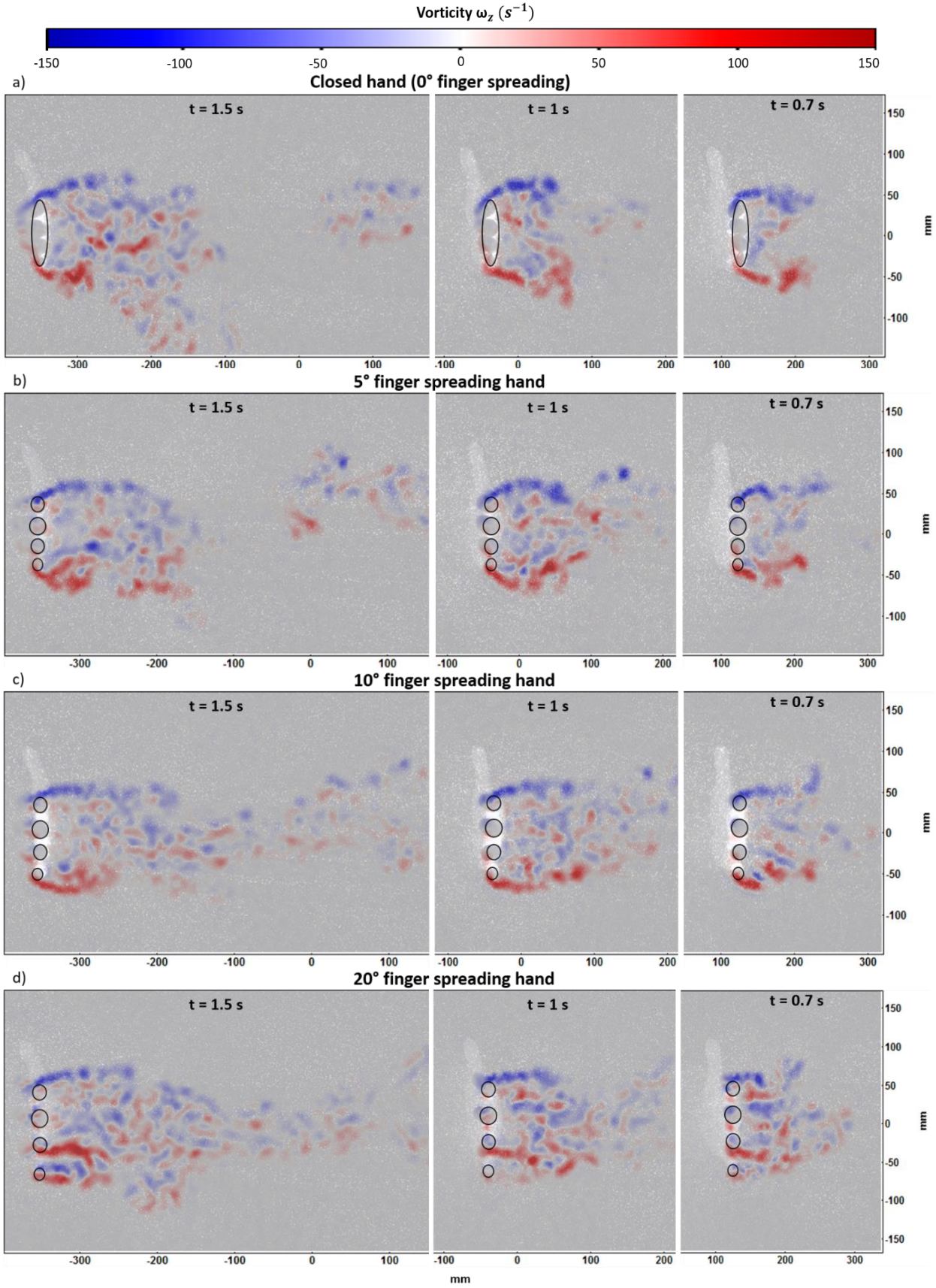

Figure 18 : Vorticity ω_z at three different times during the 1st half of the motion for the four hands a) closed hand, b) 5° finger spreading hand, c) 10° finger spreading hand and d) 20° finger spreading hand.

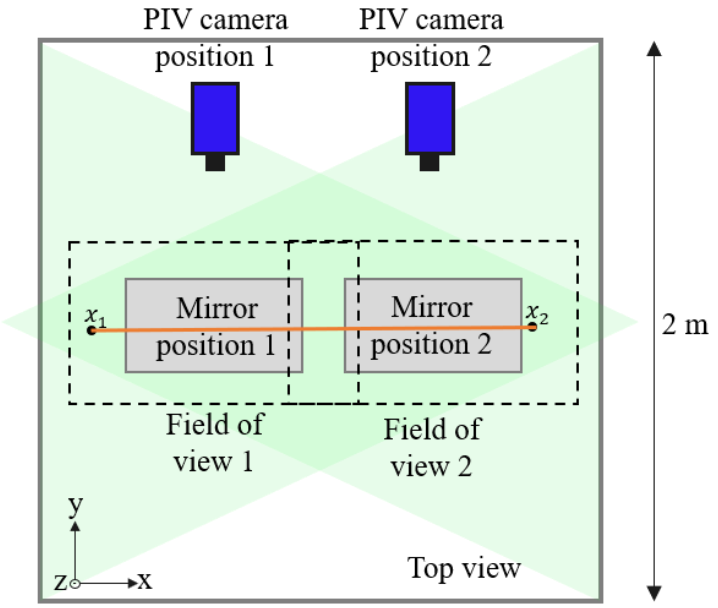

Figure 19 : Top view of the PIV set-up showing the two positions of the camera and the mirror to capture respectively the first half and the second half of the motion.

Figure 20 shows the vorticity ω_z of the closed and 5° finger spreading hands during the second part of the motion, containing the second half of the transition phase and the steady phase as explained above, for the same kinematic conditions as before. Three different times are observed, t = 1.5 s already described above, corresponding to the middle of the transition phase, t = 1.7 s during the transition phase where the difference in the drag force is the highest (see section 2.6.2) and t = 2.3 s at the end of the motion during the steady phase. At t = 1.5 s, only a small part of the wake has been captured this time, and the top-half circulation Γ+ is 20% higher for the closed hand, so there is a much larger amount of circulation close to the hand for the closed hand as previously suggested. At t = 1.7 s, one can observe again, more concentrated vortices for the closed hand compared to the 5° hand, with a 30% larger circulation Γ+, which finally leads, at t = 2.3 s, to a larger amount of vorticity behind the closed hand compared to the 5° hand and could explain the higher steady drag force obtained with the closed hand, in the same way as the flat plate (Grift et al., 2019) for the depth h = 20 mm compared to the other depths. A difference in the wake angle can be observed but unlike the flat plate (Grift et al., 2019), it appears that the hand producing the highest drag force, the closed hand, has the largest wake angle, while the 5° finger spreading hand has a smaller wake angle than the closed hand and the hand generating the lowest drag, the 10° finger spreading hand, seems to have the smallest wake angle (Figure 18).

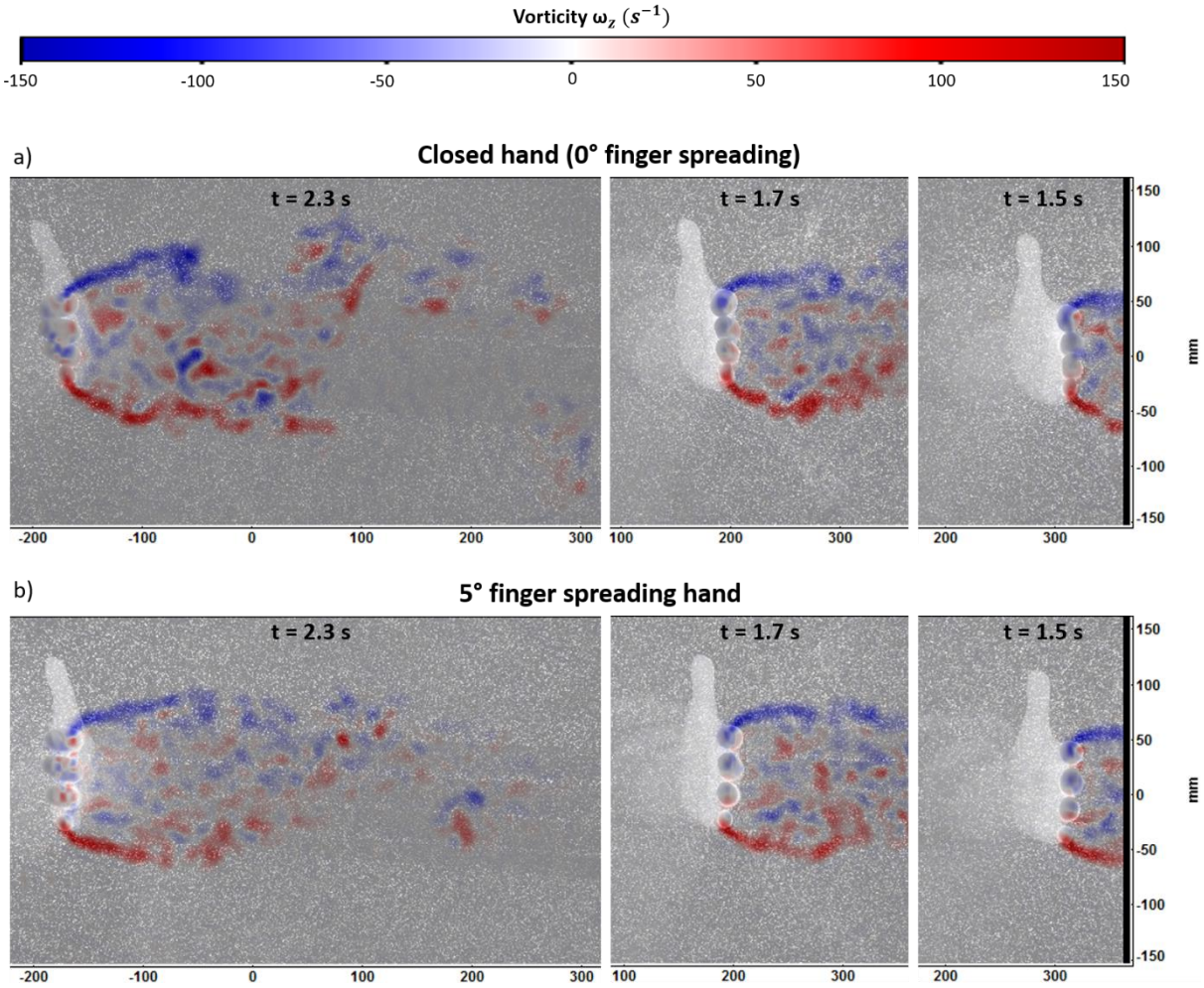

Figure 20 : Vorticity ω_z at three different times during the 2nd half of the motion for two hands a) closed hand, b) 5° finger spreading hand.

3.5. Conclusion

PIV enabled observation of the hydrodynamics around accelerating hands with different finger spreading. Despite becoming quickly turbulent, the flow around the hands on the selected plan showed a great repeatability in the hydrodynamics observed regarding the computed circulation. The comparison of different accelerations demonstrated that a higher acceleration generates a concentrated and well-defined pair of vortices close to hand while lower accelerations show a pair of vortices more dissipated and moving away from the hand. This is translated into a larger amount of circulation Γ+, based on the top-half surface S+, for a low acceleration but a much longer wake, which finally results in more circulation close to the hand for a high acceleration. This probably lead to a lower pressure behind the hand for a high acceleration, so a higher pressure difference resulting in a larger drag force exerting on the hand as found with the force measurements. The comparison of the different finger spreading showed a chaotic wake for the 20° hand as soon as the acceleration ends, especially with jets between the fingers, while the three others generate a pair of vortices. These vortices move away from the hand for the hands with a finger spreading (5° and 10°), especially the 10° hand, while they stay close to the hand for the closed hand. Finally, around the end of the

transition phase and during the steady phase, the closed hand shows a more concentrated pair of vortices followed by a larger amount of circulation closed the hand compared to the 5° finger spreading hand. These observations are most likely causing the difference observed in the drag force during the linear accelerating motion between the closed hand and the hands with finger spreading.

4. Conclusion

The aim of this study was to investigate the effect of acceleration on the propulsion drag of the hand in swimming and to quantify how this effect evolves with finger spreading. Similarly to the flat plate (Grift et al., 2019), the flow around hands accelerating at a towards a velocity V has been investigated for various finger spreading of the hand, combining force measurements with PIV. Measurements of the drag force generated by the hand's motion as a function of time has been performed. The two-dimensional flow field in a horizontal plan crossing the four fingers has been investigated by means of PIV from which the vorticity ω_z and the circulation Γ have been computed. As Grift et al., three phases have been distinguished in the force signal. Firstly, the results showed that a high acceleration generates stronger pair of vortices and a more concentrated amount of circulation behind the hand, leading to a higher drag force at the end of the acceleration compared to low accelerations. In this way, acceleration has a major effect on the propulsion drag generated by the hand in swimming, especially considering that the actual motion of the hands in front crawl does not contain steady phase, so the hands are continuously accelerating or decelerating (see Figure 2). No significant difference has been found between the four finger spreading during the acceleration phase. Secondly, during the transition phase where the velocity is constant, the drag force gradually decreases and quickly becomes independent on the acceleration, the closed hand starts to differ significantly from the hands with finger spreading, with a larger amount of circulation closed the hand leading to a higher drag force for the closed hand. Finally, the steady phase showed higher C_d for the closed hand at the different kinematic conditions tested, which differ significantly from the results in the literature.

Nevertheless, a small angle of attack with a leading thumb, for the experiments with the closed hand, has been lately noticed (see Figure 17), and it could be partly responsible of the higher drag generated by the latter (van den Berg et al., 2018) compared to hands with finger spreading. Additional experiments on the closed hand, correcting this small angle, would enable to clarify the results obtained regarding the finger spreading in this study. Also, no interaction has been clearly found between acceleration and finger spreading. Higher accelerations should be performed combined with a more adapted scaling of the hand with the velocities reached, to make dynamic experiments at more realistic swimming conditions (Re) and to investigate the interaction between acceleration and finger spreading for higher accelerations closer to actual swimming conditions. In addition, measurements or calculation of the pressure field would enable to verify certain observations made in this study. Finally, performing experiments in a larger water tank would enable to make longer run, and also more complex and realistic motion.

Investigation of the hand configuration is essential for the research of propulsion drag optimisation in human swimming. However, acceleration is omnipresent in the hand's motion, and has been revealed to be of great importance in the generation of propulsive forces in this study. Therefore, hand configuration, as well as the other parameters influencing a swimmer's propulsion, should not be dissociate from unsteady motion when investigating their effect on the hydrodynamics of swimming in order to reach higher performance.

A. Repeatability of the force measurements

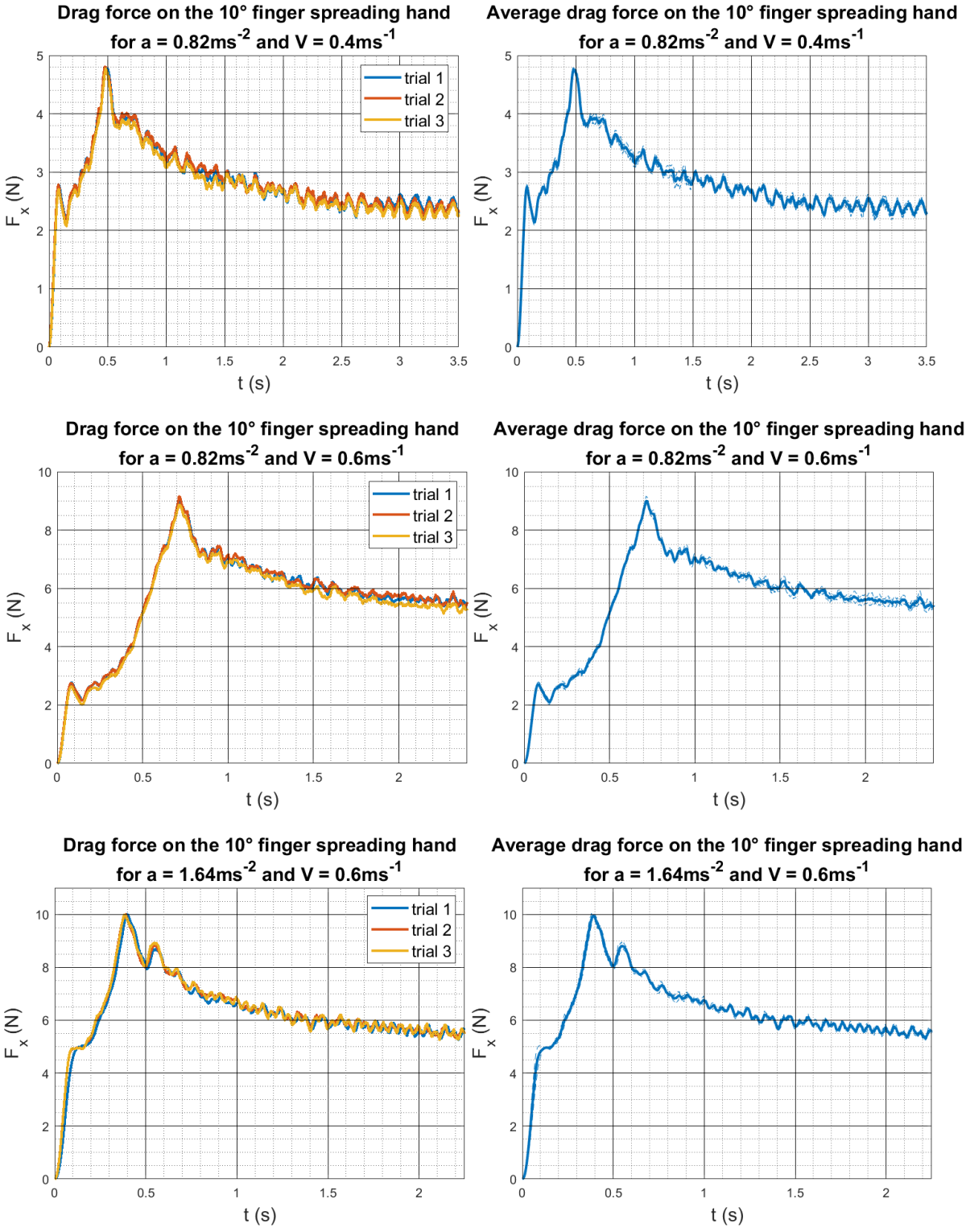

Figure 21 : Repeatability of the force measurements for two accelerations a = 0.82 ms^{-2} and a = 1.64 ms^{-2} and two target velocities V = 0.4 ms^{-1} and V = 0.6 ms^{-1} on the 10° hand. The left graph shows drag force as a function of time for the three repetitions, the right graph shows the average drag force as a function of time with the corresponding standard deviation of the data (dashed signal). The standard deviation varies with time, goes up to 3% but mostly stays below 2%.

B. Hands projected area and volume

B.1. Calculated from numerical models of the hands

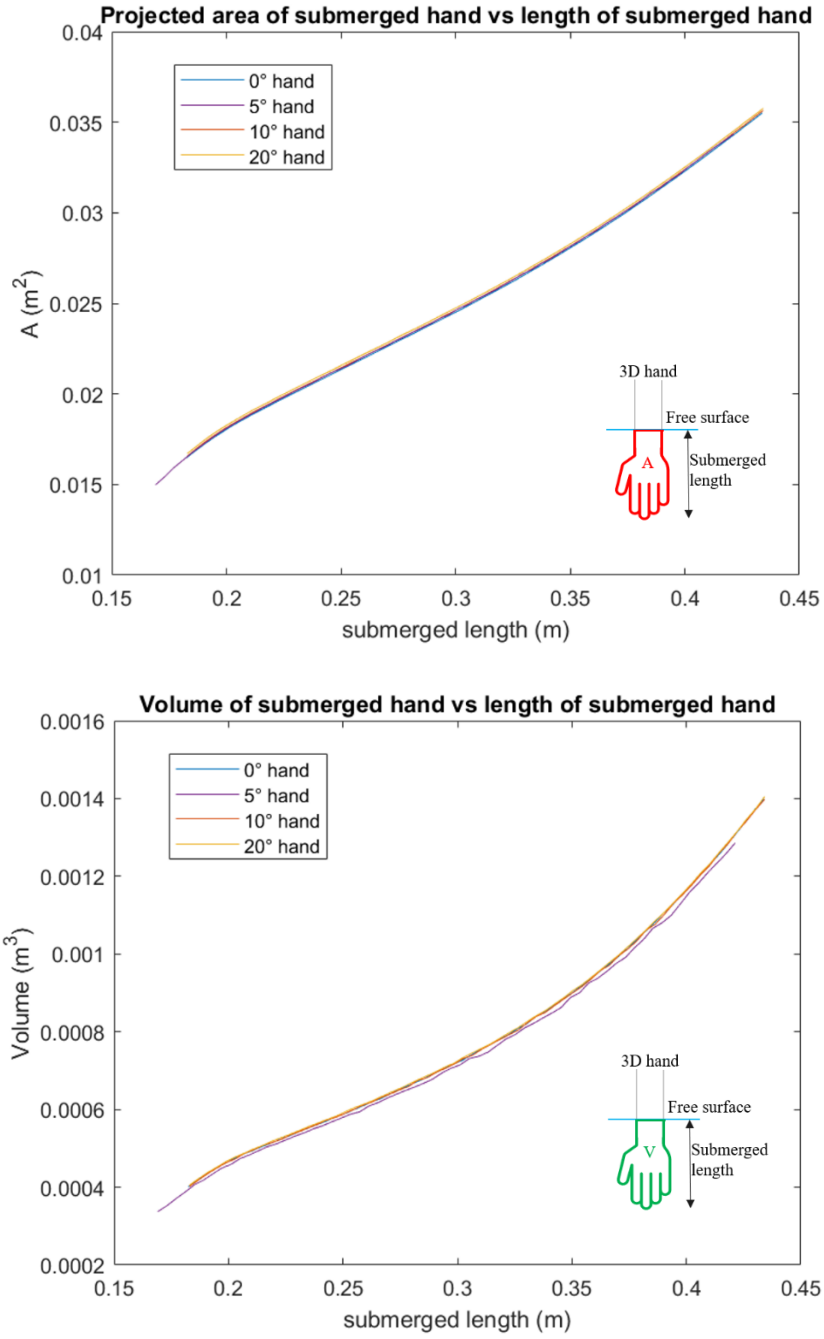

Figure 22 : Projected area and volume of the four hands, calculated from the numerical models of the hands (van Houwelingen et al., 2017b), **as a function of the submerged length, as illustrated by the scheme on the bottom right of each graph.**

One can see a small shift between the 5° hand and the three others in the range of submerged length. This is due to a different design of the 5° hand compared to the three others (the 5° hand is slightly shorter and has a different base design, see Figure 23). These differences have been considered to make sure the experiments are performed with the same conditions for the four hands, in particular with the same submerged depth. A 1% maximum difference is

observed in the projected area between the four hands for a fixed submerged length, from the numerical models.

B.2. Pictures of the hands

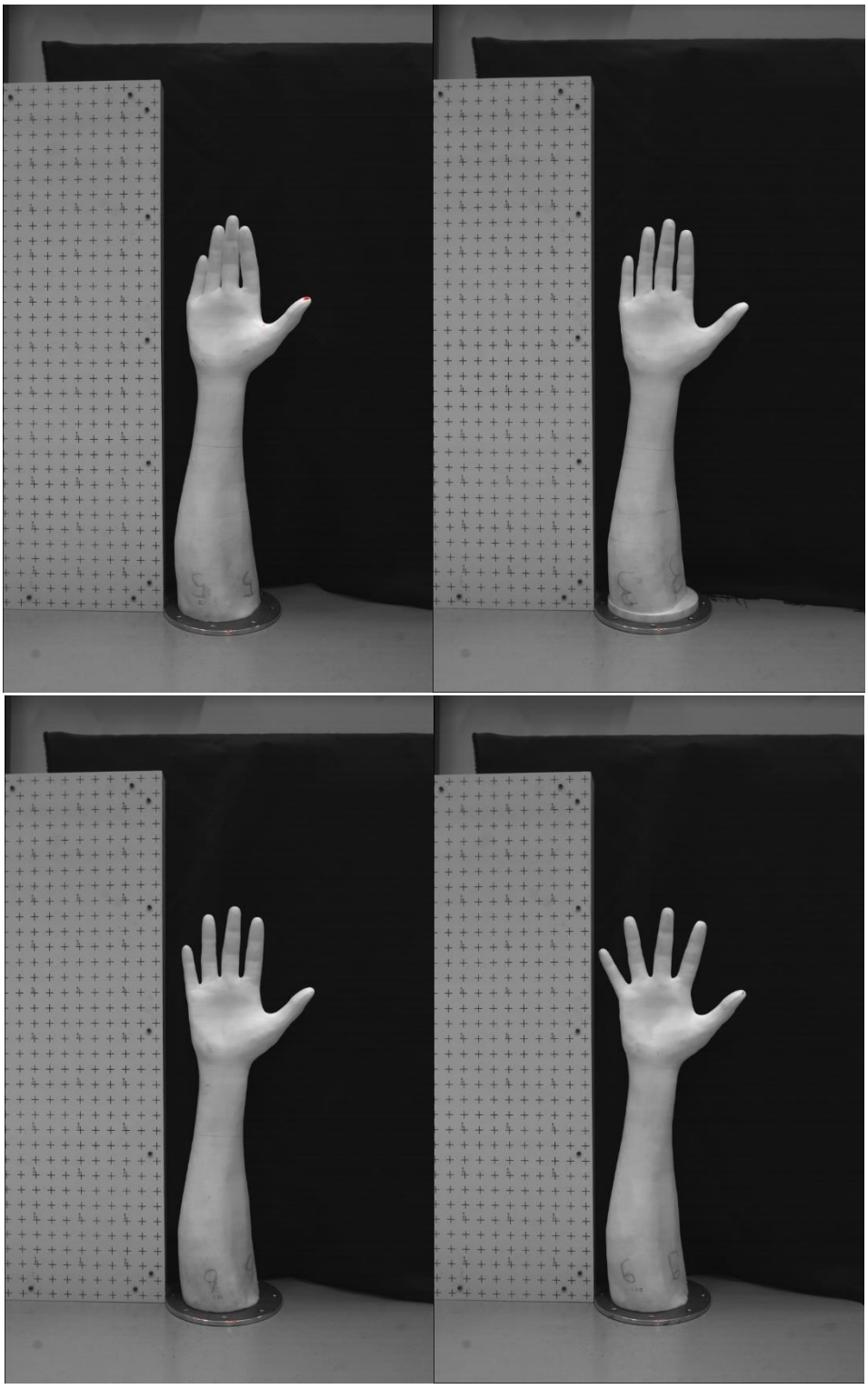

Figure 23 : Images of the four hands, next to a scaling target, used to calculate the projected area by means of image processing on Matlab (Figure 5). Respectively from top to bottom and from left to right: the closed hand, the 5° hand, the 10° hand, and the 20° hand.

C. PIV data

C.1. Repeatability of the flow dynamics

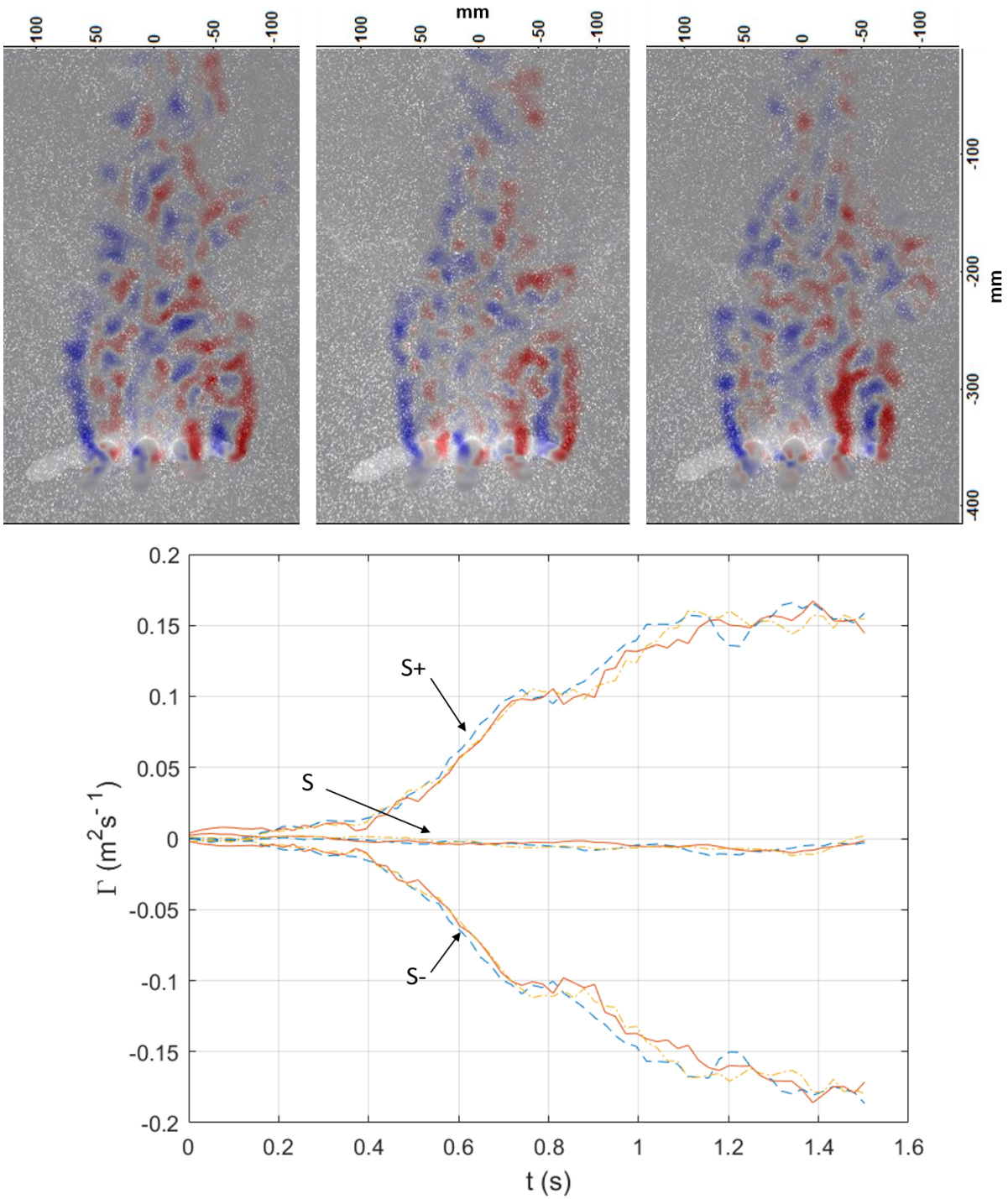

Figure 24 : Vorticity ω_z at t = 1.5 s for three realisations around the 20° finger spreading hand for a = 0.82 m/s² and V = 0.6 m/s. Below, the corresponding circulation Γ as a function of time between t = 0 s and t = 1.5 s, computed around the 20° hand for the three trials (different colours). The graph shows the circulation based on the total flow field S and the circulation based on the top-half surface S+ and the bottom-half surface S- (see Figure 16).

C.2. Circulation around the four hands

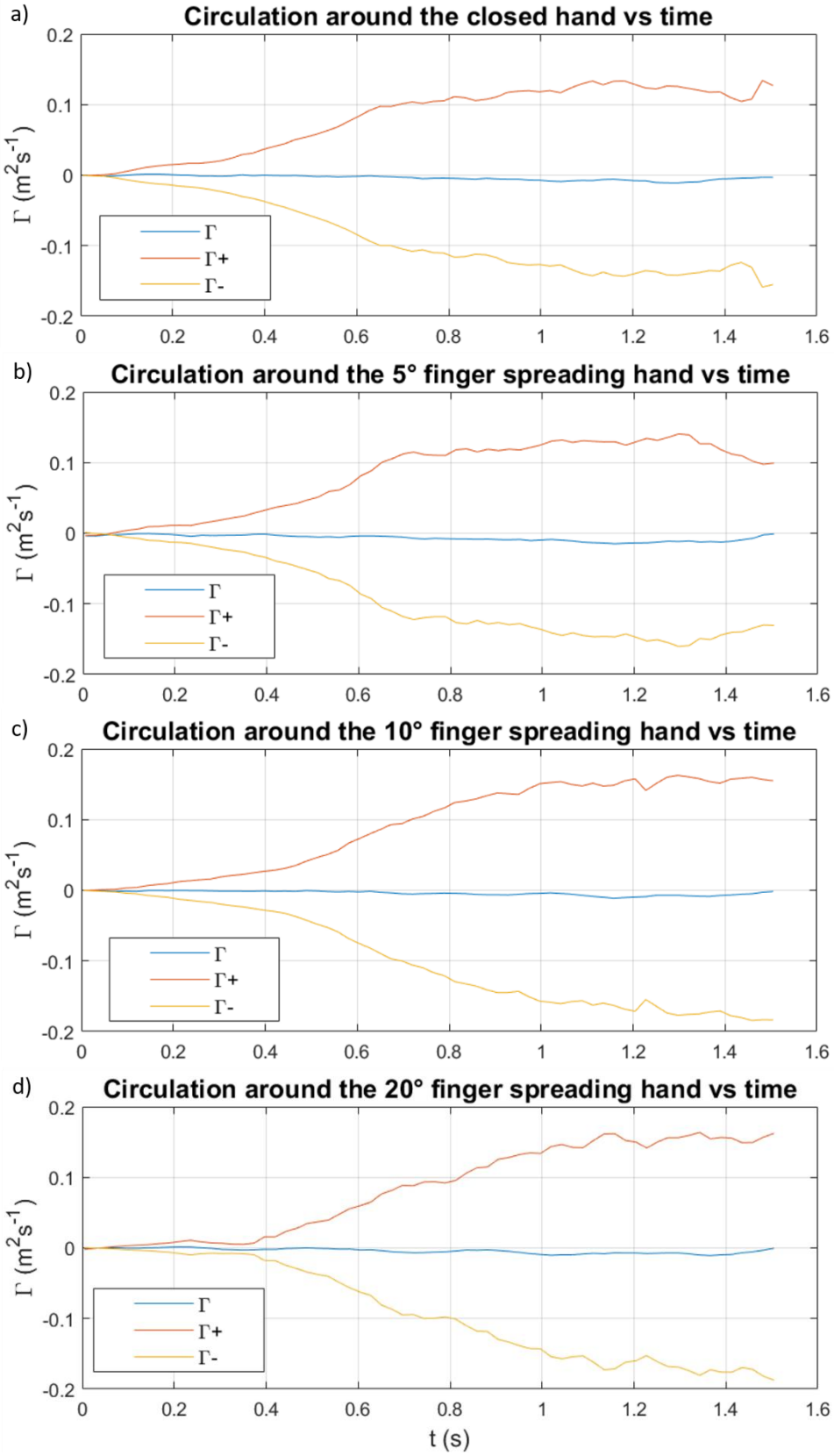

Figure 25 : Circulation as a function of time based on the total flow field S (Γ), the top-half S+ (Γ+) and the bottom-half S- (Γ-), respectively for: a) the closed hand, b) the 5° hand, c) the 10° hand and, d) the 20° hand.

Bibliography

Adrian, R. J., & Westerweel, J. (2011). *Particle image velocimetry* (W. Shyy & V. Yang, Eds.). Cambridge University Press.

Bilinauskaite, M., Mantha, V. R., Rouboa, A. I., Ziliukas, P., & Silva, A. J. (2013). Computational fluid dynamics study of swimmer's hand velocity, orientation, and shape: Contributions to hydrodynamics. *BioMed Research International*, *2013*. https://doi.org/10.1155/2013/140487

Cortesi, M., Giovanardi, A., Gatta, G., Mangia, A. L., Bartolomei, S., & Fantozzi, S. (2019). Sensors in Swimming: Detection of Stroke Phases through 3D Wrist Trajectory. In *©Journal of Sports Science and Medicine* (Vol. 18). http://www.jssm.org

Gourgoulis, V., Antoniou, P., Aggeloussis, N., Mavridis, G., Kasimatis, P., Vezos, N., Boli, A., & Mavromatis, G. (2010). Kinematic characteristics of the stroke and orientation of the hand during front crawl resisted swimming. *Journal of Sports Sciences*, *28*(11), 1165–1173. https://doi.org/10.1080/02640414.2010.507251

Gourgoulis, V., Boli, A., Aggeloussis, N., Antoniou, P., Toubekis, A., & Mavromatis, G. (2015). The influence of the hand's acceleration and the relative contribution of drag and lift forces in front crawl swimming. *Journal of Sports Sciences*, *33*(7), 696–712. https://doi.org/10.1080/02640414.2014.962571

Grift, E. J., Vijayaragavan, N. B., Tummers, M. J., & Westerweel, J. (2019). Drag force on an accelerating submerged plate. *Journal of Fluid Mechanics*, *866*, 369–398. https://doi.org/10.1017/jfm.2019.102

Keane, R. D., & Adrian, R. J. (1992). Theory of cross-correlation analysis of PIV images. In *Applied Scientific Research* (Vol. 49).

Kudo, S., Vennell, R., & Wilson, B. (2013). The effect of unsteady flow due to acceleration on hydrodynamic forces acting on the hand in swimming. *Journal of Biomechanics*, *46*(10), 1697–1704. https://doi.org/10.1016/j.jbiomech.2013.04.002

Lorente, S., Cetkin, E., Bello-Ochende, T., Meyer, J. P., & Bejan, A. (2012). The constructal-law physics of why swimmers must spread their fingers and toes. *Journal of Theoretical Biology*, *308*, 141–146. https://doi.org/10.1016/j.jtbi.2012.05.033

Marinho, D. A., Barbosa, T. M., Reis, V. M., Kjendlie, L., Alves, F. B., Vilas-Boas, J. P., Machado, L., Silva, A. J., & Rouboa, A. I. (2010). Swimming Propulsion Forces Are Enhanced by a Small Finger Spread. In *Journal of Applied Biomechanics* (Vol. 26).

Marinho, D. A., Rouboa, A. I., Alves, F. B., Vilas-Boas, J. P., Machado, L., Reis, V. M., & Silva, A. J. (2009). Hydrodynamic analysis of different thumb positions in swimming. In *©Journal of Sports Science and Medicine* (Vol. 8). http://www.jssm.org

Minetti, A. E., Machtsiras, G., & Masters, J. C. (2009). The optimum finger spacing in human swimming. *Journal of Biomechanics*. https://doi.org/10.1016/j.jbiomech.2009.06.012

Mooney, R., Corley, G., Godfrey, A., Quinlan, L. R., & ÓLaighin, G. (2015). Inertial sensor technology for elite swimming performance analysis: A systematic review. In *Sensors (Switzerland)* (Vol. 16, Issue 1). MDPI AG. https://doi.org/10.3390/s16010018

Samson, M., Bernard, A., Monnet, T., Lacouture, P., & David, L. (2017). Unsteady computational fluid dynamics in front crawl swimming. *Computer Methods in Biomechanics and Biomedical Engineering*, *20*(7), 783–793. https://doi.org/10.1080/10255842.2017.1302434

Scharnowski, S., & Kähler, C. J. (2020). Particle image velocimetry - Classical operating rules from today's perspective. In *Optics and Lasers in Engineering*. Elsevier Ltd. https://doi.org/10.1016/j.optlaseng.2020.106185

Schleihauf, R. E. (1979). *A Hydrodynamic Analysis of Swimming Propulsion*.

Takagi, H., Nakashima, M., Ozaki, T., & Matsuuchi, K. (2014a). Unsteady hydrodynamic forces acting on a robotic arm and its flow field: Application to the crawl stroke. *Journal of Biomechanics*, *47*(6). https://doi.org/10.1016/j.jbiomech.2014.01.046

Takagi, H., Shimada, S., Miwa, T., Kudo, S., Sanders, R., & Matsuuchi, K. (2014b). Unsteady hydrodynamic forces acting on a hand and its flow field during sculling motion. *Human Movement Science*. https://doi.org/10.1016/j.humov.2014.09.003

van den Berg, J., Bazuin, R., Jux, C., Sciacchitano, A., Westerweel, J., & van de Water, W. (2018). *The effect of hand posture on swimming efficiency*.

van Houwelingen, J., Schreven, S., Smeets, J. B. J., Clercx, H. J. H., & Beek, P. J. (2017a). Effective propulsion in swimming: Grasping the hydrodynamics of hand and arm movements. In *Journal of Applied Biomechanics* (Vol. 33, Issue 1, pp. 87–100). Human Kinetics Publishers Inc. https://doi.org/10.1123/jab.2016-0064

van Houwelingen, J., Willemsen, D. H. J., Kunnen, R. P. J., van Heijst, G. J. F., Grift, E. J., Breugem, W. P., Delfos, R., Westerweel, J., Clercx, H. J. H., & van de Water, W. (2017b). The effect of finger spreading on drag of the hand in human swimming. *Journal of Biomechanics*, *63*, 67–73. https://doi.org/10.1016/j.jbiomech.2017.08.002

Wei, T., Mark, R., & Hutchison, S. (2014). The Fluid Dynamics of Competitive Swimming. *Annual Review of Fluid Mechanics*, *46*(1), 547–565. https://doi.org/10.1146/annurev-fluid-011212-140658